

Observations of recent Arctic sea ice volume loss and its impact on ocean-atmosphere energy exchange and ice production

N. T. Kurtz,^{1,2} T. Markus,² S. L. Farrell,^{2,3} D. L. Worthen,^{2,4} and L. N. Boisvert^{2,5}

Received 2 March 2010; revised 3 December 2010; accepted 27 January 2011; published 16 April 2011.

[1] Using recently developed techniques we estimate snow and sea ice thickness distributions for the Arctic basin through the combination of freeboard data from the Ice, Cloud, and land Elevation Satellite (ICESat) and a snow depth model. These data are used with meteorological data and a thermodynamic sea ice model to calculate ocean-atmosphere heat exchange and ice volume production during the 2003–2008 fall and winter seasons. The calculated heat fluxes and ice growth rates are in agreement with previous observations over multiyear ice. In this study, we calculate heat fluxes and ice growth rates for the full distribution of ice thicknesses covering the Arctic basin and determine the impact of ice thickness change on the calculated values. Thinning of the sea ice is observed which greatly increases the 2005–2007 fall period ocean-atmosphere heat fluxes compared to those observed in 2003. Although there was also a decline in sea ice thickness for the winter periods, the winter time heat flux was found to be less impacted by the observed changes in ice thickness. A large increase in the net Arctic ocean-atmosphere heat output is also observed in the fall periods due to changes in the areal coverage of sea ice. The anomalously low sea ice coverage in 2007 led to a net ocean-atmosphere heat output approximately 3 times greater than was observed in previous years and suggests that sea ice losses are now playing a role in increasing surface air temperatures in the Arctic.

Citation: Kurtz, N. T., T. Markus, S. L. Farrell, D. L. Worthen, and L. N. Boisvert (2011), Observations of recent Arctic sea ice volume loss and its impact on ocean-atmosphere energy exchange and ice production, *J. Geophys. Res.*, 116, C04015, doi:10.1029/2010JC006235.

1. Introduction

[2] Recent observations have shown a decline in Arctic sea ice areal coverage, freeboard, thickness, and volume [e.g., *Stroeve et al.*, 2008; *Farrell et al.*, 2009; *Rothrock et al.*, 2008; *Giles et al.*, 2008; *Kwok et al.*, 2009] along with widespread environmental and climatic changes in the Arctic [*Arctic Climate Impact Assessment*, 2005]. These changes to the sea ice system have the potential to impact the Arctic climate by altering the radiation and heat budgets of the ocean and atmosphere. The degree to which the cold Arctic atmosphere is insulated from the relatively warm ocean is affected by the presence of a sea ice cover; the ocean-atmosphere heat flux can vary by nearly 2 orders of magnitude between open water and an ocean covered with thick sea ice for winter time conditions [*Maykut*, 1978]. This insulating

effect of sea ice makes the Arctic much colder than is typical of a maritime environment. The exchange of heat between the ocean and the atmosphere is also responsible for the growth of sea ice as heat lost from the ocean to the atmosphere is balanced by ice production. With thinner ice comes more heat exchange and faster ice growth which could potentially slow or reverse the observed losses in ice thickness.

[3] The loss of sea ice may play a role in Arctic amplification, wherein the Arctic region is expected to see a much greater share of warming as worldwide temperatures increase [*Manabe and Stouffer*, 1980]. Modeling studies show that decreases in sea ice thickness and its areal coverage lead to increased ocean-atmosphere heat transfer. Due to the strong stratification of the Arctic atmosphere this heat is trapped near the surface leading to increased surface air temperatures [*Boé et al.*, 2009]. In addition to modeling studies, observations from buoy data have suggested that thinning of the sea ice cover during the 1979–1998 time period led to increases in surface air temperature through an increase in the ocean-atmosphere heat flux [*Rigor et al.*, 2002]. There remains, however, much uncertainty into how large a role recent changes in the sea ice cover have, and will continue to play, with regard to Arctic warming. Using reanalysis data, *Serreze et al.* [2009] found that losses in sea ice areal coverage have played a role in autumn surface air temperature increases in the Arctic. They also found that a winter warming signal may be beginning to emerge which they hypothesize may be due

¹Joint Center for Earth Systems Technology, University of Maryland Baltimore County, Baltimore, Maryland, USA.

²Hydrospheric and Biospheric Sciences Laboratory, NASA Goddard Space Flight Center, Greenbelt, Maryland, USA.

³Cooperative Institute for Climate Studies, Earth System Science Interdisciplinary Center, University of Maryland, College Park, Maryland, USA.

⁴RS Information Systems, McLean, Virginia, USA.

⁵Department of Atmospheric and Oceanic Sciences, University of Maryland, College Park, Maryland, USA.

Table 1. Input Parameters Used in This Study and Their Sources

Symbol	Description	Source
T_a	2 m air temperature	ECMWF
T_d	2 m dew point temperature	ECMWF
p_0	surface pressure	ECMWF
u	10 m wind speed	ECMWF
Cl	cloud fraction	MODIS
T_w	sea surface temperature	AMSR-E
h_s	snow depth	snow model
h_f	freeboard	ICESat
h_i	ice thickness	ICESat freeboard with snow model

to delays in autumn freezeup and decreased ice extent and thickness in the winter. However, a major limitation in studies such as these has been the lack of a high-resolution, basin-wide sea ice thickness observational data set with which to adequately study the impact of sea ice thickness changes on the Arctic energy budget.

[4] Recent satellite altimetry missions have provided the capability of obtaining basin-wide Arctic sea ice thickness measurements. In this paper, we use laser altimetry data from NASA’s Ice, Cloud, and land Elevation Satellite (ICESat) to estimate sea ice freeboard across the Arctic basin. The freeboard data are then combined with a snow depth model to estimate sea ice and snow thickness values for the Arctic at the high spatial resolution needed for studying the impact of sea ice on the energy budget. The sea ice thickness data are used with meteorological data and a thermodynamic sea ice model to study the impact of sea ice thickness changes on the ocean–atmosphere heat flux and ice growth rate over the 2003–2008 time period when significant changes to the Arctic sea ice cover took place.

[5] The meteorological forcings, as well as the data sets and methodologies used to derive the sea ice thickness and snow depth are described in section 2. Section 3 describes the thermodynamic model used for determining the heat transfer through the ocean–ice–atmosphere system and calculating the ice growth rate. The calculated heat fluxes, ice growth rates, and uncertainties are presented in section 4 and compared to results from previous studies. The role of observed thinning of the ice and snow covers in increasing the ocean–atmosphere heat flux is also discussed. Section 5 expands the analysis to the full Arctic Ocean including nonice-covered regions. Section 6 summarizes the main conclusions of our study.

2. Data Sets

[6] In this section, we provide a description of the data sets and methods used to derive snow depth, sea ice thickness, and the meteorological parameters used in our analysis. These data sets are used in the following section to calculate the ocean–atmosphere heat flux and ice growth rate. No single sensor provides the requisite data, thus a combination of observation, model, and assimilated data is used. Table 1 provides a summary of the input data sets with detailed descriptions provided below. Error estimates for each data set, along with the propagation of these errors into the calculated heat flux and ice growth rate, are addressed in section 5. We restrict our data set to the Arctic Ocean region shown in the shaded region of Figure 1 to avoid mixing high- and low-latitude sea ice regions in the analysis.

2.1. Meteorological Data

[7] Reanalysis data from the European Center for Medium-Range Weather Forecasts (ECMWF) ERA-Interim data set are used to provide the 2 m air temperature, 2 m dew point temperature, 10 m wind speed, surface pressure, and snowfall. ERA-Interim combines observational and model data into an assimilated data set using the 4D-VAR method. Data is provided at 6 h time intervals with a spatial resolution of 1.5° latitude by 1.5° longitude.

[8] Cloud fraction is taken from the daily Moderate Resolution Imaging Spectroradiometer (MODIS) $1^\circ \times 1^\circ$ global gridded product. A correction factor of 0.1 has been added to all cloud fraction data to account for a bias in the Arctic region of the data set [Ackerman *et al.*, 2008]. Cloud fractions from MODIS, rather than ECMWF are used because of the anomalously high values found in the ECMWF data for this time period; the ECMWF cloud fractions were found to be approximately 30–40% higher than those from previously published observations [e.g., Lindsay, 1998].

[9] Sea surface temperatures are classified as the temperature of the top layer of water approximately 1 millimeter thick. They are taken from the daily 0.25° by 0.25° gridded product derived from ten-channel Advanced Microwave Scanning Radiometer–Earth Observing System (AMSR-E) brightness temperature data [Wentz and Meissner, 2004]. These sea surface temperatures are provided for ice-free areas to within 75 km of coastlines. The estimated error in the sea surface temperatures is 0.58 K [Wentz and Meissner, 2000].

2.2. Snow Model

[10] Snow depth on sea ice is modeled using a domain defined by the 25 km AMSR-E grid. Snow depth on the model grid is determined by

$$\frac{\partial S}{\partial t} = -\nabla \cdot (V \cdot S) + a_i \frac{\rho_s}{\rho_w} F,$$

where S is the average snow thickness in a grid cell (including both open water and ice covered areas), V is the

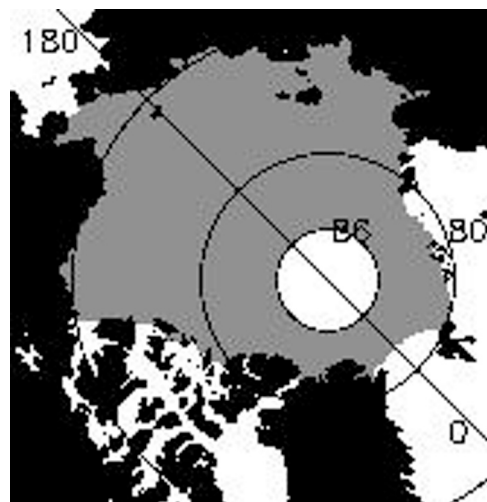


Figure 1. Map of the region used in the analysis. The shaded region is defined as the Arctic Ocean in this study.

Table 2. Time Periods Used in This Analysis Based on the Availability of ICESat Data^a

Campaign Name	Period	Days of Operation
ON03	Oct 1 to Nov 18 2003	49
ON03_1	Oct 1 to Nov 8 2003	39
ON03_2	Oct 15 to Nov 18 2003	35
FM04	Feb 17 to Mar 21 2004	34
ON04	Oct 3 to Nov 8 2004	37
FM05	Feb 17 to Mar 24 2005	36
ON05	Oct 21 to Nov 24 2005	35
FM06	Feb 22 to Mar 27 2006	34
ON06	Oct 25 to Nov 27 2006	34
MA07	Mar 12 to Apr 14 2007	34
ON07	Oct 2 to Nov 5 2007	37
FM08	Feb 17 to Mar 21 2008	34

^aThe ON03 campaign has been subdivided into two campaigns, ON03_1 and ON03_2, for better temporal comparison with other fall ICESat campaigns.

ice velocity vector, a_i is the ice concentration, ρ_s is the snow density, ρ_w is the density of water, and F is the snowfall (in snow water equivalent). The snow depth is initialized each year on 15 September before the summer minimum sea ice extent, the initial snow cover on multiyear ice and the snow density values are taken from the climatology of *Warren et al.* [1999]. The daily AMSR-E sea ice concentrations at each grid point are specified at the start of each day and remain constant throughout the day. Daily snowfall at each model grid point is estimated using the liquid water equivalent from the ECMWF ERA-Interim reanalysis data similar to the method used by *Kwok and Cunningham* [2008]. Ice velocity for each grid point is determined from AMSR-E 89 GHz data using the wavelet analysis algorithm of *Liu and Cavalieri* [1998]. The model is run each year during the fall through spring periods to estimate the snow depth over the time period covering each ICESat measurement campaign.

2.3. ICESat Data

[11] ICESat measures the surface elevation using a 1064 nm laser altimeter [*Zwally et al.*, 2002]. Spatial coverage of the Arctic Ocean is provided up to 86°N with a 170 m shot-to-shot spacing and a footprint size of approximately 70 m. The cloud filtering parameters described by *Kwok et al.* [2007] are first used to filter out low-quality data which has been affected by atmospheric forward scattering. The elevation data from ICESat are used to determine the sea ice freeboard, h_f , which is here defined as the height of the snow and ice layer above the local sea surface. Freeboard data is collected only in areas where the ice concentration determined from AMSR-E is greater than 30%. The ICESat data products are of Release 428, which include orbit and attitude determination as well as detector saturation corrections for the time periods studied here. Freeboard is found from the ICESat elevation data through the use of sea surface tie points following the method of *Kwok et al.* [2007].

[12] Due to the approximately 70 m footprint size of ICESat, some sea surface tie points used in the retrieval of freeboard from ICESat data are expected to be biased due to contamination of snow and ice within the footprint. Comparisons of ICESat data with coincident high-resolution airborne laser altimetry data have shown this can be problematic with a freeboard bias of up to 9 cm observed in one study

[*Kurtz et al.*, 2008]. Corrections to account for biases due to snow and ice within sea surface tie point footprints have been proposed by *Kwok and Cunningham* [2008] and *Kwok et al.* [2009] and are applied here in the determination of freeboard. The correction for snow depth biases are taken from *Kwok and Cunningham* [2008] which relates the albedo dependence of snow depth to the surface reflectivity measured by ICESat. An additional correction to account for remaining residual biases due to contamination of snow and ice within the ICESat footprint is taken from *Kwok et al.* [2009].

[13] The temporal sampling of ICESat is limited to the times shown in Table 2 which restricts our analysis to time periods when ICESat data is available. Throughout we will refer to ICESat campaigns by their campaign name shown in Table 2, the first two letters of the campaign name refer to the months of measurement while the numerals refer to the year (e.g., ON03 for the October–November 2003 campaign). The length of the ON03 campaign made it suitable to split into two subcampaigns for the purposes of comparing the heat flux and ice growth rates between years. The ON03_1 campaign is at a similar time of year to the ON04 and ON07 campaigns while the ON03_2 campaign is at a similar time of year to the ON05 and ON06 campaigns. The FM04, FM05, FM06, and FM08 ICESat campaigns occurred during roughly the same time of year while the MA07 campaign occurred later in the ice growth season than all other campaigns.

2.4. Sea Ice Thickness and Snow Depth

[14] The sea ice thickness, h_i , is calculated by assuming local hydrostatic balance and is given by

$$h_i = \frac{\rho_w}{\rho_w - \rho_i} h_f - \frac{\rho_w - \rho_s}{\rho_w - \rho_i} h_s, \quad (1)$$

where h_f is the height of the snow and ice layers above the water level, h_s is the snow depth, $\rho_w = 1024 \text{ kg m}^{-3}$ is the density of sea water, ρ_i is the density of sea ice taken to be 915 kg m^{-3} [*Weeks and Lee*, 1958; *Wadhams et al.*, 1992], and ρ_s is the density of snow. ρ_s is taken to be changing with time following the climatological values compiled by *Warren et al.* [1999], it varies from a minimum of 260 kg m^{-3} in early October to a maximum of 330 kg m^{-3} at the end of the winter ICESat campaigns.

[15] The large difference between the spatial resolutions of the freeboard (approximately 70 m) and snow depth (25 km) data sets leads to ambiguities when combining these data to estimate sea ice thickness. Due to the nonlinear dependence of the heat flux values on snow and ice thickness (an example of which can be seen in Figure 2 for typical winter time conditions), it is necessary to use a high spatial resolution estimate of the thickness values to properly include the contributions of thin, young ice regions which can be present in any area due to ice dynamics. *Kurtz et al.* [2009] found that the mean heat flux and ice growth values calculated for the Arctic basin using the full 70 m spatial resolution of ICESat were approximately one-third higher than those calculated using 25 km mean thickness values. Therefore, the method developed by *Kurtz et al.* [2009] for combining low-resolution snow depth data with high-resolution freeboard data is used to estimate the snow and ice thickness distributions for each of $25 \times 25 \text{ km}$ grid cells in the Arctic

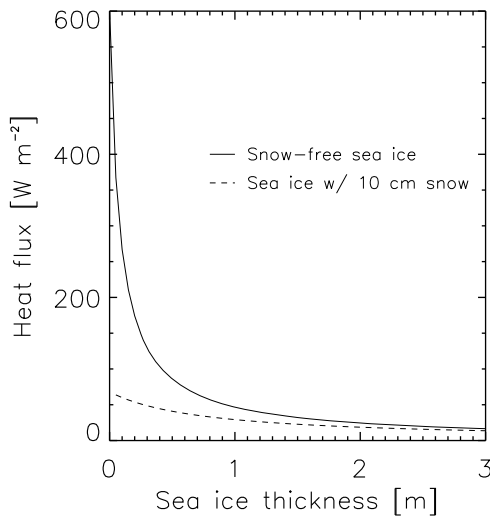


Figure 2. Plot of the dependence of the ocean-atmosphere heat flux on sea ice thickness for snow-free and snow-covered sea ice using typical winter time conditions in the Arctic. Input parameters are as follows: air temperature of -25°C , cloud fraction of 0.5, wind speed of 6 m/s, relative humidity of 0.9, and no shortwave flux.

containing available ICESat freeboard data. The method is based on an observed linear relationship between freeboard and snow depth for thin ice. The linear relationship between freeboard and snow depth applies to points with a freeboard less than a certain cutoff value, fb_{cutoff} . fb_{cutoff} is defined as

$$fb_{cutoff} = 0.69\langle h_s \rangle + 0.22\langle h_f \rangle + 5.10,$$

where $\langle h_s \rangle$ is the mean snow depth of the region which is given by the 25 km resolution snow depth model, $\langle h_f \rangle$ is the mean freeboard of the ICESat data line within the 25 km snow depth grid cell, and the units of the constant, 5.10, are in cm. A constant snow depth is used for thick ice (where $h_f > fb_{cutoff}$) and is given by

$$h_{s_{thick}} = 1.03\langle h_s \rangle + 0.83,$$

where the units of the constant value, 0.83, are also in cm. h_s is thus given by

$$h_s = \begin{cases} h_{s_{thick}} \left(\frac{h_f}{fb_{cutoff}} \right) & h_f \leq fb_{cutoff} \\ h_{s_{thick}} & h_f > fb_{cutoff} \end{cases}.$$

Here h_f is taken from the ICESat data set, and h_i is then calculated for each freeboard data point using equation 1. The ice thickness distribution for each 25×25 km grid cell is then estimated from the approximately 70 m resolution ice thickness data. A minimum of 70 freeboard points (about half the grid cell coverage) are required for the determination of the ice thickness distribution in each grid cell.

3. Thermodynamic Sea Ice Model

[16] The ocean-atmosphere heat fluxes and ice growth rates are calculated here through the use of a thermodynamic model with inputs from the data sets described in section 2.

The discrete ICESat ice and snow thickness data points are assumed to represent the thickness distribution in each model grid cell, and the heat flux and ice growth values are calculated for each individual ice thickness data point in a grid cell containing a valid number of measurements. Heat transfer between the ocean, ice, snow, and atmosphere is governed by the temperature of each system, the temperatures of the ocean and atmosphere are specified, while the temperature profiles of the ice and snow are calculated. The temperature of the ocean layer in contact with the ice is taken to be near the freezing point of seawater at $T_b = 271.35$ K, while the surface air temperature and other relevant meteorological parameters are taken from the ECMWF, AMSR-E, and MODIS data discussed in section 2. Temperature gradients are mainly vertical, therefore disregarding horizontal heat fluxes the temperature distribution within the snow and ice layers is governed by the one-dimensional heat diffusion equations

$$\rho_s c_{snow} \frac{\partial T}{\partial t} = k_s \frac{\partial^2 T}{\partial z^2}, \quad (2)$$

$$\rho_i c_{ice} \frac{\partial T}{\partial t} = k_i \frac{\partial^2 T}{\partial z^2}, \quad (3)$$

where $c_{snow} = 2.1 \times 10^3$ J kg $^{-1}$ K $^{-1}$ and $c_{ice} = 2.1 \times 10^3$ J kg $^{-1}$ K $^{-1}$ are the specific heats of ice and snow, and $k_s = 0.31$ W m $^{-1}$ K $^{-1}$ and $k_i = 2.04$ W m $^{-1}$ K $^{-1}$ are the thermal conductivities of snow and sea ice, respectively, which are empirical values obtained from *Maykut and Untersteiner* [1969]. A more recent study by *Sturm et al.* [2002] also found the effective thermal conductivity for snow to be approximately 0.3 W m $^{-1}$ K $^{-1}$. The numerical scheme used to solve equations 2 and 3 follows the three-layer model of *Semtner* [1976] with parameterizations for the individual heat flux terms described in detail below.

[17] The resultant mean surface air temperature, ocean-atmosphere heat flux, and ice growth rates used in sections 4 and 5 are the model average values over each ICESat measurement time period. They were calculated by running the thermodynamic model with 6 h time steps over each specific time period shown in Table 2. The initial temperature profiles of the snow and ice layers were determined by first setting the system in thermodynamic equilibrium then running the model over a one week time period prior to the start of each campaign shown in Table 2.

3.1. Heat Flux Parameterizations

[18] The various heat flux terms are calculated by solving the energy balance equation to find the surface temperature, T_0 , based on the method of *Maykut* [1978]. The energy balance equation at the surface is

$$F_r + F_L - F_E + F_s + F_e + F_c = 0, \quad (4)$$

where F_r is the net absorbed surface shortwave flux, F_L the incoming longwave flux, F_E the emitted longwave flux, F_s the sensible heat flux, F_e the latent heat flux, and F_c the conductive heat flux. A positive flux is defined as being toward the surface while a negative flux is away from the surface.

[19] The net absorbed shortwave flux, F_r , can be written as

$$F_r = F_{r_0}(1 - \alpha)(1 - i_0), \quad (5)$$

where F_{r_0} is the shortwave flux reaching the surface, α is the surface albedo, and i_0 is the percentage of shortwave radiation which passes through the surface and into the water. For snow covered ice α is 0.8 and i_0 is 0. For ice with a negligible snow cover (<1 cm thick is treated here as snow free) α is a function of ice thickness, h_i , and calculated using the empirical relation between ice thickness and albedo described by *Weller* [1972]. i_0 is estimated from radiative transfer calculations described by *Maykut* [1982].

[20] Many parameterizations of the F_{r_0} and F_L radiative flux terms have been proposed in the literature. *Key et al.* [1996] analyzed various schemes and found that the shortwave parameterization scheme of *Shine* [1984] and the downwelling longwave parameterization scheme of *Maykut and Church* [1973] perform well for Arctic conditions. F_{r_0} is calculated here following *Parkinson and Washington* [1979] by applying the cloudiness factor of *Laevastu* [1960] to the empirical equation of F_{r_0} for clear skies described by *Shine* [1984]. The downwelling longwave parameterization scheme of *Maykut and Church* [1973] is used to calculate F_L .

[21] The emitted longwave radiation, F_E , is given by

$$F_E = \epsilon \sigma T_0^4, \quad (6)$$

where ϵ is the longwave emissivity of the surface layer taken to be 0.99, σ is the Stefan-Boltzmann constant, and T_0 is the temperature of the surface layer.

[22] The turbulent fluxes are calculated using bulk aerodynamic formulas following *Pease* [1987]

$$F_s = \rho c_p C_s u (T_a - T_0), \quad (7)$$

$$F_e = \rho L C_e u (q_a - q_0), \quad (8)$$

where ρ is the air density, $c_p = 1004 \text{ J kg}^{-1} \text{ K}^{-1}$ is the specific heat of air at constant pressure, $C_s = 2 \times 10^{-3}$ and $C_e = 2 \times 10^{-3}$ are the sensible and latent heat transfer coefficients, respectively, for neutrally stratified air and are adjusted for unstable conditions following *Hack et al.* [1993], u is the average wind speed, $L = 2.83 \times 10^6 \text{ J kg}^{-1}$ is the latent heat of sublimation, and q is the specific humidity. The conductive flux, F_c , is calculated by following the three-layer model of *Semtner* [1976]. Three vertical grid points are used: one in the snow layer, and two evenly spaced grid points in the ice layer. The surface energy balance equation (equation 4) can now be rewritten through substitution of the parameterizations for F_r , F_L , F_E , F_s , F_e , and F_c . The surface temperature-dependent terms in the surface energy balance equation are linearized to determine the temperature change of the surface layer for each time step. A time step of 6 h is used to coincide with the temporal resolution of the input ECMWF meteorological data described in section 2. Due to the coarse resolution of the temperature grid, a forward differencing scheme is used to calculate the conductive fluxes across the snow and ice layers and find the temperature profile, which is assumed to be linear between interior grid points. The forward differencing scheme is stable for vertical grid points with $h_i > 22$ cm and $h_s > 14$ cm,

so the number of grid points is reduced as needed to maintain computational stability. For the case of ice with a thickness less than 22 cm, the “zero layer” method of *Semtner* [1976] is used to determine the vertical temperature profile, the snow and ice layers are treated as a single system that maintains thermodynamic equilibrium with the external conditions at all times.

[23] The ocean-atmosphere heat flux is defined as the net heat transferred from the ocean to the atmosphere, or $-F_c$. For open water areas, the individual heat flux terms are calculated using the above relations for F_r , F_L , F_E , F_s , and F_e with suitable changes to α , i_0 , T_0 , and L . The surface albedo of open water is taken to be 0.08 while i_0 is the amount of shortwave energy passing through the ocean mixed layer which is calculated to be 0.2 based on the results of *Maykut and Perovich* [1987] for a 30 m mixed ocean layer. The latent heat of sublimation, L , is replaced by the latent heat of vaporization which is $2.5 \times 10^6 \text{ J kg}^{-1}$. The surface temperature, T_0 , is replaced by the ocean surface temperature, T_w . T_w is taken to be constant at 271.35 K for ice-covered regions. The net ocean-atmosphere heat flux is

$$F_O = F_E - F_r - F_L - F_s - F_e. \quad (9)$$

3.2. Thermodynamic Ice Growth Rate

[24] Ablation and accretion of ice at the bottom of the sea ice layer occurs when there is an imbalance between the conductive flux through the bottom of the ice (F_{cn}) and the flux of energy from the water to the ice (F_O^{\uparrow}). The thermodynamic basal ice growth rate is calculated as

$$\frac{dh_i}{dt} = \frac{1}{Q_i} (F_{cn} - F_O^{\uparrow}), \quad (10)$$

where $Q_i = 3.02 \times 10^8 \text{ J m}^{-3}$ is the heat of fusion of ice, F_O^{\uparrow} is estimated to be $2 \pm 1 \text{ W m}^{-2}$ from the results of *Steele and Boyd* [1998], and F_{cn} is the conductive flux through the lowest ice grid point. The thermodynamic growth rate is calculated only to estimate the mean rate of ice growth for the observed ICESat thickness distributions, it is not used to change the thickness of the ice with time.

4. Results for the Ice-Covered Arctic Ocean

[25] The results presented in this section are for the sea ice covered region of the Arctic Ocean containing valid ICESat data. The ocean-atmosphere heat fluxes and ice growth rates represent approximately a monthly mean value for the study region.

4.1. Heat Flux and Ice Growth in Regions Containing ICESat Data

[26] Changes in the percentage distribution of different Arctic sea ice thickness classes over the 2003–2008 time period are shown in Figure 3 for both the fall and winter time periods. A general thinning of the ice cover is observed due to the loss of ice with thickness greater than 3 m. This is consistent with recent studies showing much of the older, thicker multiyear ice cover of the Arctic being replaced with thinner first year ice [*Maslanik et al.*, 2007; *Comiso et al.*, 2008]. Using similar data sets and methods, *Kwok et al.*

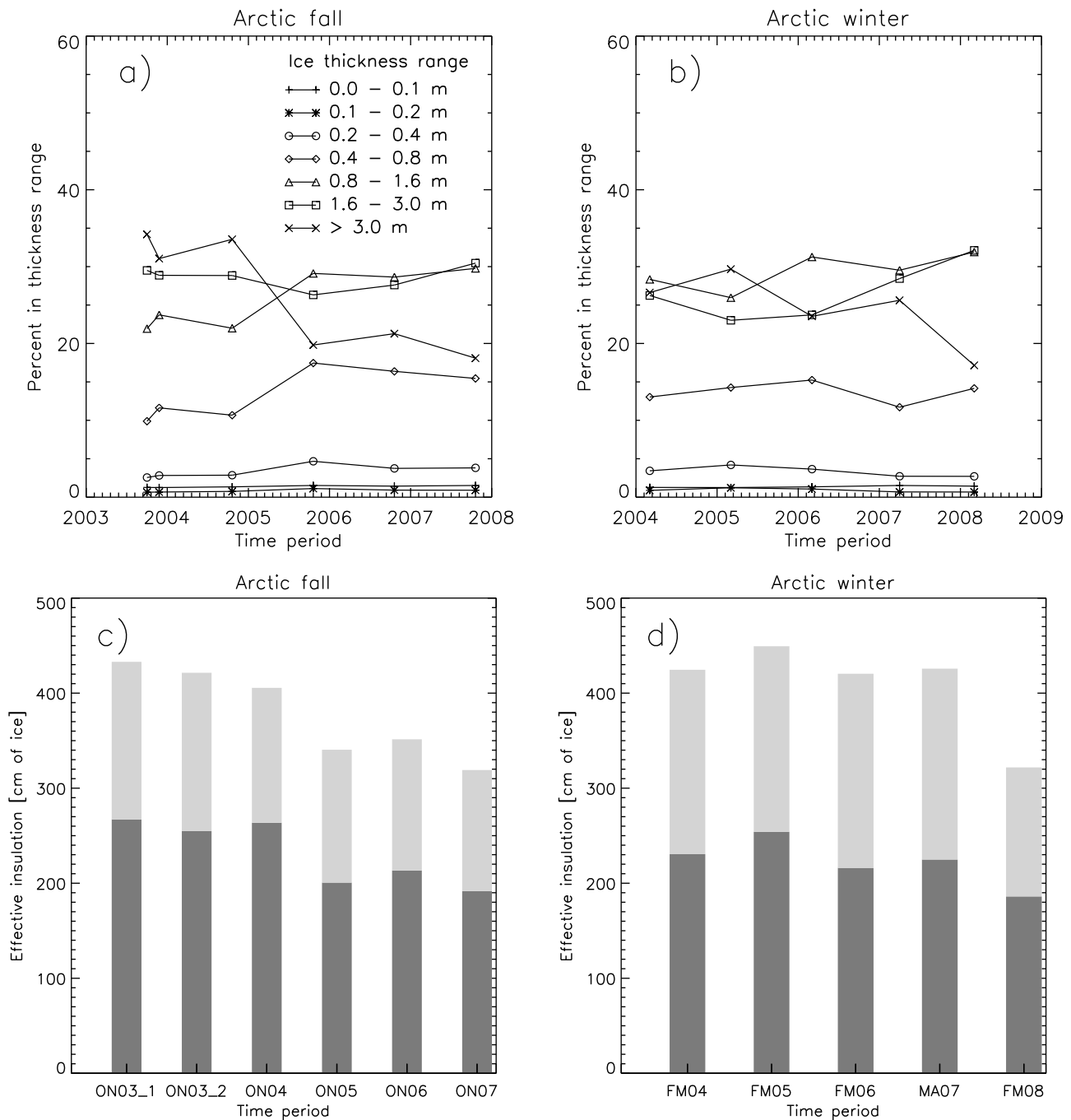


Figure 3. Distribution of ice thickness classes over the Arctic basin for the (a) fall and (b) winter ICESat campaigns. (c and d) The mean effective insulation of the snow plus sea ice cover in terms of an equivalent thickness of snow-free sea ice is also shown. The dark colored bars in Figures 3c and 3d represent the sea ice contribution, while the lighter colored bars represent the snow depth contribution.

[2009] showed a comparable thinning of the Arctic sea ice cover with an overall decrease in the mean thickness over the same time period. The sea ice thickness results shown here differ from those of *Kwok et al.* [2009] due mainly to differences in the sea ice density used (*Kwok et al.* [2009] used $\rho_i = 925 \text{ kg m}^{-3}$ while this study uses $\rho_i = 915 \text{ kg m}^{-3}$). *Wadhams et al.* [1992] summarize the results of numerous field measurements from the 1950s through the 1970s which suggest the mean density of sea ice is typically within the

range $910\text{--}920 \text{ kg m}^{-3}$ for first year ice and $910\text{--}915 \text{ kg m}^{-3}$ for multiyear ice. However, whether the density of sea ice has changed with time due to changing ice conditions is an important, but unknown factor in the determination of sea ice thickness. Errors in the calculated heat flux and ice growth rates due to uncertainty in sea ice density are discussed in section 5. Figure 3 also shows the changes that occurred to the mean effective insulation of the sea ice cover over this time period. The effective insulation is defined here as the

thermal insulating strength of the snow plus sea ice layer in terms of an equivalent thickness of snow-free sea ice, it is calculated as $h_{eff} = h_i + \frac{k_i}{k_s} h_s$. The effective insulation of the fall ice pack decreased significantly in 2005 then remained relatively constant. The loss in the effective insulation during the fall periods is associated mainly with thinning of the sea ice rather than a loss of snow. During the winter time periods, the effective insulation stayed relatively constant until 2008 when it decreased by approximately 1 m (Figure 3). This decrease in the winter of 2008 is due to thinning of both the sea ice and snow covers which is associated with the large loss in multiyear ice and record minimum sea ice extent observed in 2007.

[27] The percentage of ice within a given ice thickness class and the area weighted heat flux values for the various thickness classes are shown in Table 3. Also shown in Table 3 are the following mean input parameters: 2 m air temperature, cloud fraction, wind speed, and the calculated surface temperature. The calculated values are for areas where freeboard data from ICESat were available which can be seen in Figures 4 and 5. Areas without ICESat data were not considered in the analysis in this section.

[28] Table 3 shows that over half of the ice production and ocean-atmosphere heat flux ($-F_c$) in the ice-covered regions of the Arctic Ocean occurred over areas with an ice thickness less than 80 cm. In particular, open water and newly refrozen leads with an ice thickness less than 10 cm accounted for nearly one-third of the ocean-atmosphere heat flux and ice production within ice-covered areas. The thickest ice (>1.6 m) is the dominant ice type and was found to make up 50–60% of the total observed ice in the Arctic. Yet, the thickest ice accounted for only 20–30% of the observed ice production and ocean-atmosphere heat flux. The basin wide averaged ice growth rate was generally higher in the winter than in the fall, this was due to the lower surface air temperatures and increased area of first year ice during the winter periods. The percentage contribution of each thickness class to ice production and heat flux varied due to the changing ice thickness distributions and input meteorological parameters. The net radiative flux showed the highest variability of the radiative, turbulent, and conductive heat fluxes. However, if we exclude the anomalous MA07 time period from comparison (which had a higher net radiative flux due to the increased shortwave flux of the later spring period) the net radiation was almost constant and varied by only 4 W m^{-2} . The loss of radiative energy by the atmosphere was observed to be much stronger over areas of thick ice rather than thin ice. The sensible heat flux was quite variable with variations of 8 W m^{-2} seen during the study period. It acted to transfer heat from the surface to the atmosphere over relatively warm, thin ice ($h_i < 0.4 \text{ m}$), while over ice thicker than 0.4 m, it transferred heat from the atmosphere to the surface. Overall, the sensible heat flux was positive owing to the large areas of thick ice in the Arctic, this resulted in a net sensible heat gain by the ice. The latent heat flux varied by 2 W m^{-2} for all time periods and was generally a source of small but steady heat input to the atmosphere.

[29] The input forcings and calculated heat flux values from this study are compared with results and observations from studies by Lindsay [1998], Maykut [1982], and Persson *et al.* [2002] in Table 4. The results shown in Table 4 for

this study represent the mean over sea ice 2.75–3.25 m thick to best correspond with the observations conducted on multiyear ice floes in the comparison studies. The computed heat fluxes and forcing parameters derived in this study are within the range of observational values, with the exception of the sensible heat flux and surface air temperature, which were found to be slightly higher during the fall periods. We also compare our results for ice growth rates with those observed during the Surface Heat Budget of the Arctic Ocean (SHEBA) experiment. Perovich *et al.* [2003] studied basal ice growth rates for a 1.75 m thick multiyear ice floe (“Quebec site”) which grew to about 2.25 m thick between early October and March 1998. They report growth rates of $0.10\text{--}0.30 \text{ cm d}^{-1}$ in the fall and $0.25\text{--}0.50 \text{ cm d}^{-1}$ in the winter (at comparable times to the fall and winter ICESat campaigns shown in Table 2). For a similar ice thickness class (ice of thickness between 1.75 and 2.25 m), we obtained similar Arctic-wide growth rates of $0.19\text{--}0.32 \text{ cm d}^{-1}$ (mean 0.24 cm d^{-1}) in the fall and $0.27\text{--}0.44 \text{ cm d}^{-1}$ (mean 0.33 cm d^{-1}) in the winter. These comparisons demonstrate reasonable agreement between our derived results and observations from previous studies. The major advantage of the remote sensing data sets used here is that it is now possible to calculate the ocean-atmosphere heat flux and ice growth rate for all ice-covered areas of the Arctic. Table 3 thus expands on the knowledge from previous observational studies by providing information over the full range of ice thickness classes of the Arctic Ocean.

[30] Maps of the mean effective insulation, surface air temperature, ocean-atmosphere heat flux, and ice growth rate are shown in Figure 4 for the fall time periods and Figure 5 for the winter time periods. Figures 4 and 5 show that there was great spatial and temporal variability in the effective insulation, air temperature, heat flux, and ice growth rate during the study period. An analysis of the variability in the heat flux and ice growth rate, due to losses in the effective insulation coupled with changes in the meteorological forcings, is the subject of section 4.2.

4.2. Analysis of Heat Flux and Ice Growth Variability

[31] The mean values for the ocean-atmosphere heat fluxes and ice growth rates in Table 3 do not show a clear correlation between an increased ocean-atmosphere heat flux/growth rate and the observed decrease in ice thickness and snow depth derived from the ICESat and snow model data sets. This follows since the observed heat flux also depends on the various meteorological forcings with the surface air temperature playing the largest role. Since surface air temperatures in the Arctic tend to be highly variable, it is likely that any trend in the heat flux values over this short 5 year time period is masked by the natural variability caused by variations in the surface air temperature.

[32] The goal of this section is to better understand the causes of the variability that occurred over the study period. That is, we seek to determine whether the observed variability of the heat flux and ice growth is due mainly to changes in meteorological conditions, changes in ice and snow thickness, or uncertainties in the input parameters. First, we first determine the uncertainty in the heat flux and ice growth rates through estimation of the errors in the input parameters. Next we run the thermodynamic model for each time period using constant meteorological forcings to focus

Table 3. Thickness Distribution Averages, Ice Production, and Heat Flux Values Over the Ice-Covered Regions of the Arctic Ocean^a

Thickness Category	ON03_1	ON03_2	FM04	ON04	FM05	ON05	FM06	ON06	MA07	ON07	FM08
<i>Percentage of Ice in Each Thickness Category</i>											
0–0.1 m	1.3	1.3	1.4	1.3	1.7	1.5	1.5	1.4	1.3	1.5	1.3
0.1–0.2 m	0.6	0.7	0.9	0.8	1.2	1.1	1.1	0.9	0.7	0.9	0.7
0.2–0.4 m	2.6	2.8	3.4	2.9	4.2	4.7	3.6	3.7	2.7	3.8	2.7
0.4–0.8 m	9.9	11.6	13.0	10.7	14.3	17.5	15.2	16.4	11.7	15.4	14.2
0.8–1.6 m	21.9	23.7	28.3	22.0	26.0	29.1	31.3	28.6	29.5	29.8	31.9
1.6–3.0 m	29.5	28.9	26.2	28.8	23.0	26.3	23.7	27.6	28.4	30.5	32.1
≥3.0	34.2	31.0	26.6	33.6	29.7	19.8	23.5	21.3	25.6	18.1	17.2
<i>Net Radiation $F_r + F_L - F_E$ ($W m^{-2}$)</i>											
0–0.1 m	-1.1	-1.3	-1.6	-1.2	-1.6	-1.4	-1.4	-1.4	-0.8	-1.2	-1.4
0.1–0.2 m	-0.3	-0.3	-0.4	-0.3	-0.5	-0.5	-0.5	-0.4	-0.2	-0.4	-0.3
0.2–0.4 m	-0.9	-1.1	-1.3	-1.0	-1.5	-1.8	-1.4	-1.2	-0.7	-1.3	-1.0
0.4–0.8 m	-3.1	-3.9	-4.2	-3.3	-4.6	-5.9	-5.1	-4.8	-2.8	-5.0	-4.8
0.8–1.6 m	-6.1	-6.9	-8.3	-6.3	-7.5	-8.8	-9.1	-7.6	-6.2	-8.8	-9.7
1.6–∞	-14.3	-13.7	-12.8	-14.6	-12.1	-11.3	-10.8	-10.8	-8.7	-12.2	-12.7
Total	-25.8	-27.1	-28.6	-26.7	-27.7	-29.8	-28.2	-26.1	-19.4	-28.9	-29.9
<i>Sensible Heat Flux F_s ($W m^{-2}$)</i>											
0–0.1 m	-2.7	-3.0	-4.8	-3.0	-4.3	-3.4	-4.1	-3.7	-3.1	-2.5	-3.8
0.1–0.2 m	-0.2	-0.3	-0.5	-0.2	-0.5	-0.3	-0.4	-0.4	-0.2	-0.1	-0.4
0.2–0.4 m	0.0	-0.2	-0.6	-0.2	-0.4	-0.2	-0.2	-0.5	-0.1	0.3	-0.4
0.4–0.8 m	1.0	0.8	0.3	0.8	1.0	1.5	1.7	0.4	0.9	2.2	0.5
0.8–1.6 m	2.9	2.6	3.2	2.6	3.3	3.6	4.5	2.4	3.3	4.7	3.4
1.6–∞	7.0	6.0	6.5	6.9	6.3	5.5	6.0	4.9	5.3	6.8	6.0
Total	7.9	6.0	4.1	6.9	5.3	6.6	7.6	3.2	6.1	11.4	5.3
<i>Latent Heat Flux F_e ($W m^{-2}$)</i>											
0–0.1 m	-1.0	-0.9	-1.3	-1.0	-1.3	-1.2	-1.3	-1.2	-1.1	-1.0	-1.1
0.1–0.2 m	-0.1	-0.1	-0.1	-0.1	-0.2	-0.1	-0.1	-0.1	-0.1	-0.1	-0.1
0.2–0.4 m	-0.1	-0.1	-0.2	-0.2	-0.3	-0.3	-0.3	-0.3	-0.3	-0.2	-0.2
0.4–0.8 m	-0.2	-0.2	-0.4	-0.3	-0.5	-0.4	-0.6	-0.5	-0.6	-0.2	-0.5
0.8–1.6 m	0.0	0.0	-0.3	-0.1	-0.3	-0.2	-0.4	-0.4	-0.6	0.0	-0.6
1.6–∞	0.6	0.3	0.0	0.4	0.1	0.2	0.0	0.1	-0.2	0.6	-0.2
Total	-0.8	-1.0	-2.4	-1.3	-2.6	-2.0	-2.6	-2.4	-2.8	-0.9	-2.7
<i>Conductive Heat Flux F_c ($W m^{-2}$)</i>											
0–0.1 m	4.8	5.2	7.6	5.2	7.1	6.0	6.7	6.2	4.9	4.7	6.3
0.1–0.2 m	0.5	0.6	1.0	0.6	1.2	1.0	1.0	0.9	0.5	0.5	0.8
0.2–0.4 m	1.1	1.4	2.1	1.3	2.3	2.2	1.8	1.9	1.1	1.3	1.7
0.4–0.8 m	2.3	3.3	4.3	2.8	4.2	4.9	4.0	4.9	2.4	3.1	4.7
0.8–1.6 m	3.3	4.3	5.5	3.8	4.5	5.4	4.9	5.6	3.6	4.1	6.8
1.6–∞	6.7	7.4	6.3	7.3	5.7	5.6	4.8	5.8	3.6	4.7	7.0
Total	18.7	22.2	26.9	21.0	25.0	25.2	23.2	25.3	16.2	18.4	27.2
<i>Ice Growth Rate ($cm month^{-1}$)</i>											
0–0.1 m	4.1	4.4	6.5	4.5	6.1	5.1	5.8	5.3	4.2	4.0	5.4
0.1–0.2 m	0.4	0.5	0.9	0.5	1.0	0.8	0.8	0.7	0.4	0.5	0.6
0.2–0.4 m	0.9	1.1	1.8	1.1	1.9	1.8	1.5	1.6	0.9	1.0	1.4
0.4–0.8 m	1.7	2.5	3.5	2.1	3.3	3.8	3.1	3.8	2.0	2.2	3.8
0.8–1.6 m	2.0	2.8	4.2	2.3	3.3	3.8	3.6	4.0	3.1	2.5	5.4
1.6–∞	2.5	3.3	4.6	3.1	3.2	3.1	3.2	3.4	3.8	2.2	5.6
Total	11.6	14.7	21.6	13.6	18.8	18.5	18.0	18.9	14.4	12.5	22.2
<i>Mean Input Parameters</i>											
$\langle T_a \rangle$ (K)	253.8	250.2	244.5	252.9	248.3	251.7	249.1	250.8	253.3	257.8	246.6
$\langle T_s \rangle$ (K)	251.8	248.2	242.7	251.0	246.3	250.2	247.0	249.7	251.8	256.0	245.1
$\langle Cl \rangle$	0.64	0.58	0.42	0.61	0.48	0.58	0.44	0.67	0.55	0.65	0.45
$\langle u \rangle$ ($m s^{-1}$)	6.2	5.5	6.2	6.0	6.3	6.2	6.5	6.2	6.8	6.7	5.7

^aThe heat fluxes and ice production rates for the different ice thickness categories have been weighted by the percentage of ice within each respective thickness category.

exclusively on how the observed changes to the sea ice and snow thickness distributions affected the heat flux and growth rates across the Arctic ice pack.

4.2.1. Sensitivity to Input Parameter Uncertainties

[33] We now estimate the sensitivities and uncertainties in the heat flux and growth rate due to variations in the input parameters. To determine the impact of variability in

the input parameters on the heat flux and ice growth rate, the thermodynamic model was run multiple times to simulate variations in each individual parameter separately over a range of values. The goal was to calculate the sensitivities of the heat flux ($\frac{\partial F_c}{\partial x}$) and ice growth rate ($\frac{\partial g_{growth}}{\partial x}$) to the input parameters (x), and estimate an uncertainty value by multiplying the sensitivity by the estimated uncertainty, σ_x . Sea-

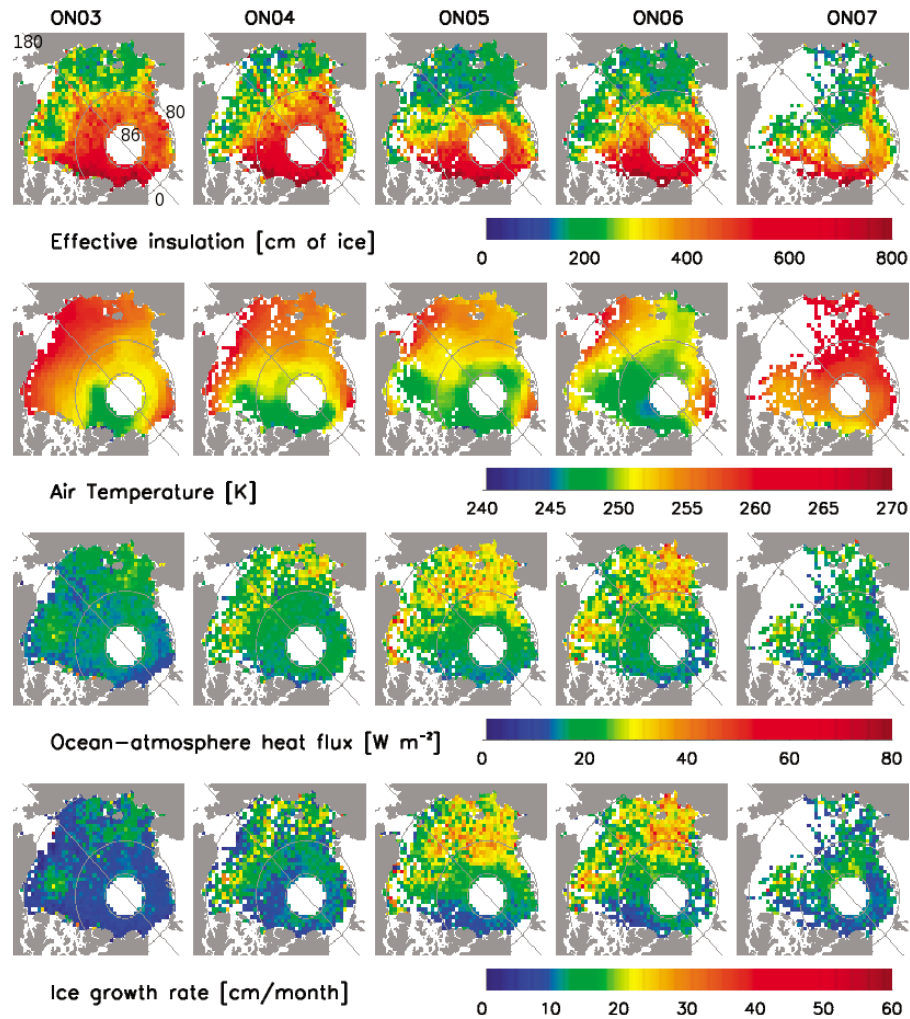


Figure 4. Map of the effective insulation, snow depth, and air temperature parameters and the calculated ocean-atmosphere heat fluxes and ice growth rates for the fall measurement periods.

sonal sensitivities were calculated and used in the estimation of the uncertainties of the heat fluxes and ice growth rates in section 4.2.2. Average values of the calculated sensitivities and estimated uncertainties for the fall and winter time periods are shown in Table 5. In the following discussion, only the freeboard uncertainties are assumed to be from a zero mean random process. All other error sources are not well constrained, thus the net error estimates σ_{F_e} and σ_{growth} presented in Table 5 are RSS errors calculated from the individual error terms.

[34] Estimating uncertainties for the meteorological input parameters is challenging since errors in the ECMWF Interim surface air temperature, and wind speed for the Arctic have not been adequately determined at this time. For sea ice covered regions, the ECMWF meteorological parameters are modeled assuming a uniform snow-free 1.5 m thick ice slab, ice concentration is considered using a blend of model and observation data [Stark *et al.*, 2007]. As shown in Figures 4 and 5, the assumption of a uniform effective ice thickness of 1.5 m is typically not valid which may impact the ECMWF model results. The uncertainties in the ECMWF data depend not only on the model accuracy, but also on the quantity and

quality of observations used in the assimilation which can vary considerably in time and space. Here we estimate the uncertainties in these values by assuming that they represent 50% of the maximum observed variability of the areal mean across similar time periods. For example, the mean surface air temperature of the ice-covered Arctic, $\langle T_a \rangle$, varied from 253.3–257.9 K between the ON03_1, ON04, and ON07 campaigns leading to an observed variability of 4.6 K and an estimated uncertainty of 2.3 K. Similarly, uncertainties of 0.6 m/s were estimated for the wind speed. Lupkes *et al.* [2010] compared ECMWF Interim near surface air temperatures and wind speeds to data from several ship cruises in the late summer in the Arctic and found a warm bias of 1.5–2 K in the Interim temperature data set and near zero error in the wind speed. While this bias in the summer data may not apply to the fall and winter time periods used in this study, it suggests that our uncertainties for the surface air temperature and wind speed may be a reasonable estimate. However, the uncertainty in the surface air temperature may vary regionally as it depends on the number of observations used in the assimilation. Additionally, the low resolution of the ECMWF data could potentially lead to errors near the ice

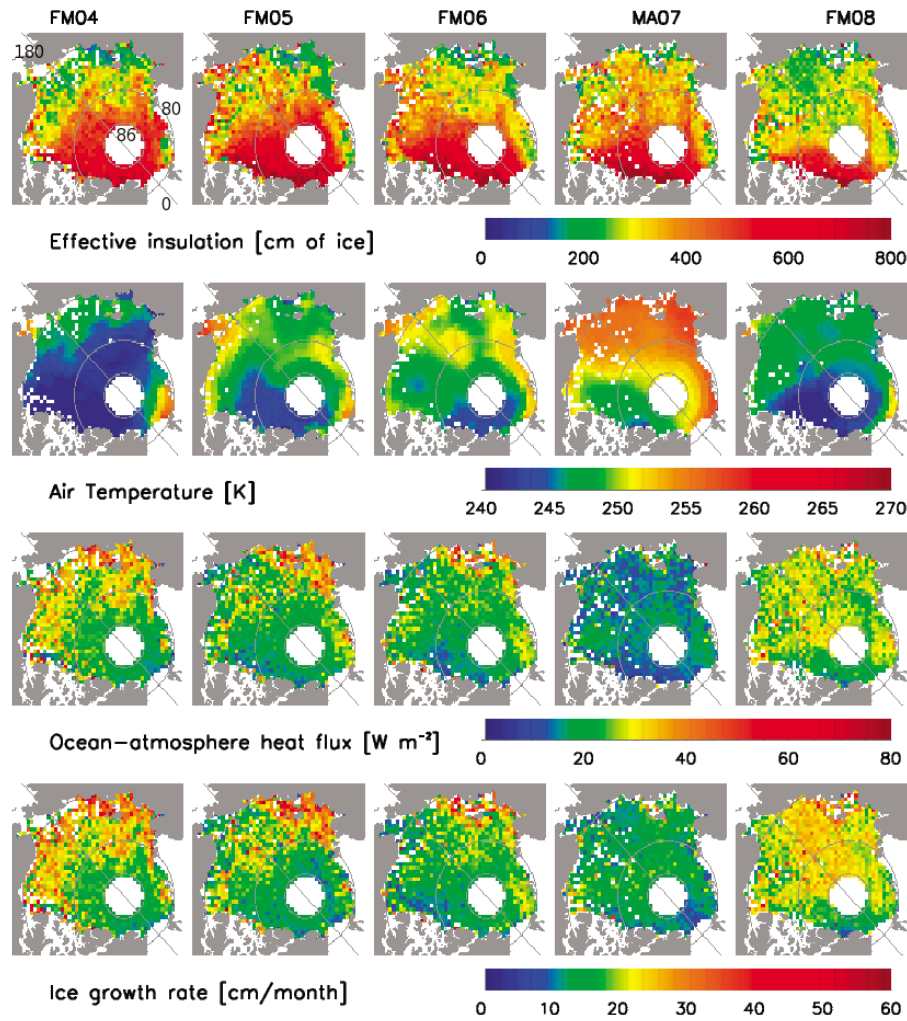


Figure 5. Map of the effective insulation, snow depth, and air temperature parameters and the calculated ocean-atmosphere heat fluxes and ice growth rates for the winter and early spring measurement periods.

edge. Errors in the MODIS cloud fractions are estimated to be 0.1 for the Arctic region based on a study by *Ackerman et al.* [2008].

[35] Errors in the ice thickness and snow depth input parameters are due to uncertainties in the freeboard, snow depth, and density values. Errors in the freeboard were

assumed to be unbiased (after the corrections for biases due to snow and ice contamination were applied) but estimated to have a random normally distributed error of $\sigma_{fb_{si}} = 5$ cm [*Kwok and Cunningham, 2008*]. σ_{ρ_i} is estimated to be 10 kg m^{-3} which represents the range of expected densities for sea ice between 0.3 and 3 m thick [*Kovacs, 1996*]. σ_{ρ_s} is

Table 4. Comparison of Heat Flux and Forcing Parameters for the Mean of All 2.75–3.25 m Thick Ice Areas With Observations^a

Parameter	This Study (2.75–3.25 m Ice Only)	L98	M82	P02
	Net radiation	−22 (−23)	−24 (−26)	−23 (−18)
F_s	12 (11)	8 (4)	12 (5)	5 (5)
F_e	0 (1)	1 (0)	0 (−2)	−1 (1)
F_c	11 (11)	—	11 (14)	6 (10)
T_a (K)	248 (252)	241 (250)	242 (249)	251 (250)
u (m s^{-1})	6 (6)	4 (4)	5 (5)	5 (7)
CI	0.5 (0.6)	0.5 (0.6)	—	—

^aObservations are from *Lindsay* [1998] (L98), *Maykut* [1982] (M82), and *Persson et al.* [2002] (P02). Values from M82 are taken from the 3 m ice thickness results. Values for the fall time periods are in parentheses, while those for the winter are not.

Table 5. Sensitivity of the Ocean-Atmosphere Heat Flux and Ice Growth Rate to Variations in the Input Parameters^a

x	σ_x	Heat Flux (W m^{-2})		Growth Rate (cm month^{-1})	
		$\frac{\partial F_c}{\partial x}$	$\sigma_x \frac{\partial F_c}{\partial x}$	$\frac{\partial \text{growth}}{\partial x}$	$\sigma_x \frac{\partial \text{growth}}{\partial x}$
T_a (K)	2.3	1.1(1.0)	2.5(2.3)	0.9(0.8)	2.1(1.8)
CI (%)	10	0.02(0.01)	0.2(0.1)	0.02(0.01)	0.2(0.1)
u (m s^{-1})	0.6	0.8(0.8)	0.5(0.5)	0.7(0.7)	0.4(0.4)
fb_{si} (cm)	5	0.3(0.3)	1.6(1.5)	0.3(0.3)	1.4(1.3)
h_s (cm)	5	0.02(0.01)	0.09(0.04)	0.02(0.01)	0.08(0.04)
ρ_i (kg m^{-3})	10	0.1(0.1)	0.9(0.8)	0.1(0.1)	0.8(0.7)
ρ_s (kg m^{-3})	100	0.01(0.01)	0.7(1.2)	0.01(0.01)	0.6(1.0)
F_0^i (W m^{-2})	1	—	—	0.9	0.9(0.9)
σ_{F_c}	—	—	3.3(3.2)	—	—
σ_{growth}	—	—	—	—	2.8(2.7)

^aResults for the winter time periods are in parentheses.

estimated to be 100 kg/m^3 based on the variability of ρ_s in the climatology of *Warren et al.* [1999]. Uncertainties and sensitivities due to variations in the density of sea water, dew point temperature (humidity), and surface air pressure are small and not considered here. Errors in the snow depth are unknown and estimated to be 5 cm here, but this value will be shown to be of small importance in the following discussion.

[36] Table 5 shows that most of the uncertainty in both the heat flux and ice growth values is due to the relatively large uncertainty estimated for T_a with lesser contributions due to uncertainty associated with sea ice freeboard, cloud fraction, wind speed, snow density, and ice density. Errors due to snow depth uncertainties are minor and contribute little to uncertainties in the heat flux and growth rates since errors in the snow depth are nearly canceled by the corresponding retrieval errors in ice thickness. Essentially, 1 cm of snow has an effective insulation of $k_i/k_s = 6.5 \text{ cm}$ of ice, while a 1 cm error in snow depth leads to a corresponding error of $\frac{\rho_w - \rho_s}{\rho_w} \approx 6.5 \text{ cm}$ in ice thickness which makes errors due to snow depth uncertainties small. In this assessment, errors in the calculated mean heat flux and ice growth rate values for the Arctic are primarily due to errors in T_a . However, changes in the cloud cover and associated incoming longwave radiation can also lead to changes in the surface air temperature which cannot be studied with a simple model such as the one used here. Aside from the impacts to surface air temperature, cloud cover changes are not a strong source of variability in the sensitivity of the ice growth rate and heat flux values. To better estimate the errors in the heat fluxes and ice growth rates calculated here, additional studies of the error in the ECMWF data for T_a in the Arctic during the fall and winter time periods are needed. The next largest source of error is due to freeboard uncertainties, these errors are due to instrumental uncertainties and set a lower limit for the total uncertainty in the calculated heat flux and ice growth rate.

4.2.2. Heat Flux Variability in Ice-Covered Regions

[37] The sensitivity results for the various meteorological forcings shown in Table 5 demonstrate that changes in T_a are much more dominant than Cl and u in affecting variability in the calculated heat fluxes and ice growth rates. Variability in the surface air temperature is therefore one of the main factors that must be considered in analyzing the observed variability in the ocean-atmosphere heat flux and ice growth rate. Figure 6 shows the mean ocean-atmosphere heat flux and ice growth rate for the ice-covered Arctic Ocean over the different time periods as well as the corresponding mean surface air temperatures. The observed heat fluxes and growth rate values can be seen to primarily change with variations in the surface air temperature. However, the changes in the ON05, ON06, ON07, and FM08 time periods are disproportionate compared to earlier changes in T_a . The ON05 and ON06 heat fluxes were much higher than those observed during the ON03_2 time period despite the higher surface air temperatures. Similarly, the winter FM08 time period has a higher heat flux than the FM04 time period despite a higher surface air temperature of 2.1 K. Figure 3 shows that there was a significant change in ice thickness distribution and an associated large decline in the effective insulation during these time periods. The percentage of ice with a thickness greater than 3 m experienced the greatest decline beginning around the fall of 2005 and this was

accompanied by an increase in the percentage of 0.4–1.6 m ice in the fall and 0.8–1.6 m ice in the winter. As shown in Figure 2, the ocean-atmosphere heat flux is sensitive to changes in the percentage of thin ice, especially for ice less than approximately 1 m thick. The percentage of the thinnest ice classes (<0.4 m) did not change significantly over the 2003–2008 time period, however this value is reported for the ice-covered Arctic only and does not take into account the large changes in open water and loss of ice area for the entire Arctic also observed during this time period.

[38] The FM05 and FM06 time periods have similar mean growth rates, heat fluxes, and surface air temperatures (Figures 6b and 6d) even though there was a decline in the percentage of thick ice during this time and a decline in mean ice thickness of 38 cm. The decrease in the percentage of the ice >3 m thick was compensated by an increase in the percentage of ice 1.6–3.0 m thick (Figure 3b). Since the ocean-atmosphere heat flux and ice growth are much less sensitive to changes for ice in this thickness range it appears that variability in heat flux and ice growth during these winter time periods was dominated more by variability in the surface air temperature. The MA07 heat flux and growth rate is much lower than the other winter time periods, this is likely due to the higher surface air temperatures resulting from the later date of data collection as well as thicker ice cover due to the longer time available for sea ice growth.

[39] The full effect of the observed increase in the ocean-atmosphere heat flux due to a thinning of the ice and snow cover is difficult to quantify since the ocean-atmosphere heat flux and surface air temperature are coupled. The ocean-atmosphere heat flux will increase with decreasing temperature and vice versa until an equilibrium is reached between the surface heat flux and other factors (such as atmospheric energy transport) which determine the surface air temperature. Nevertheless, to investigate the effect of changes in the snow and ice thickness distribution on the observed heat flux values (independent of changes due to meteorological conditions), we ran the thermodynamic model for the ice and snow thickness distributions for each individual time period using the same fixed meteorological conditions. Figure 7 shows the ocean-atmosphere heat flux differences for the individual time periods under the same meteorological conditions relative to the first campaign of the fall or winter season. This shows that thinning of the sea ice and snow covers led to potential ocean-atmosphere heat flux increases of nearly 6 W m^{-2} for the fall 2005–2007 time periods compared to the 2003 time period (an increase of approximately 40% over the heat flux observed in ON03_1). Despite the similarly large decrease in the effective insulation observed in ON05 and FM08 (Figure 3), the FM08 ocean-atmosphere heat flux would only be 2 W m^{-2} higher than FM04 under equivalent meteorological conditions (an increase of approximately 10% from the observed heat flux in FM08), but this is also within the uncertainty of the values.

[40] The results show that the observed thinning of sea ice during the 2005–2008 time period led to large increases in the ocean-atmosphere heat fluxes for the subsequent fall periods. The increased ocean-atmosphere heat flux likely impacted the surface air temperatures and may have played a part in the surface air temperature anomalies observed during this same period by *Serreze et al.* [2009]. The winter results suggest that despite losses in ice thickness and

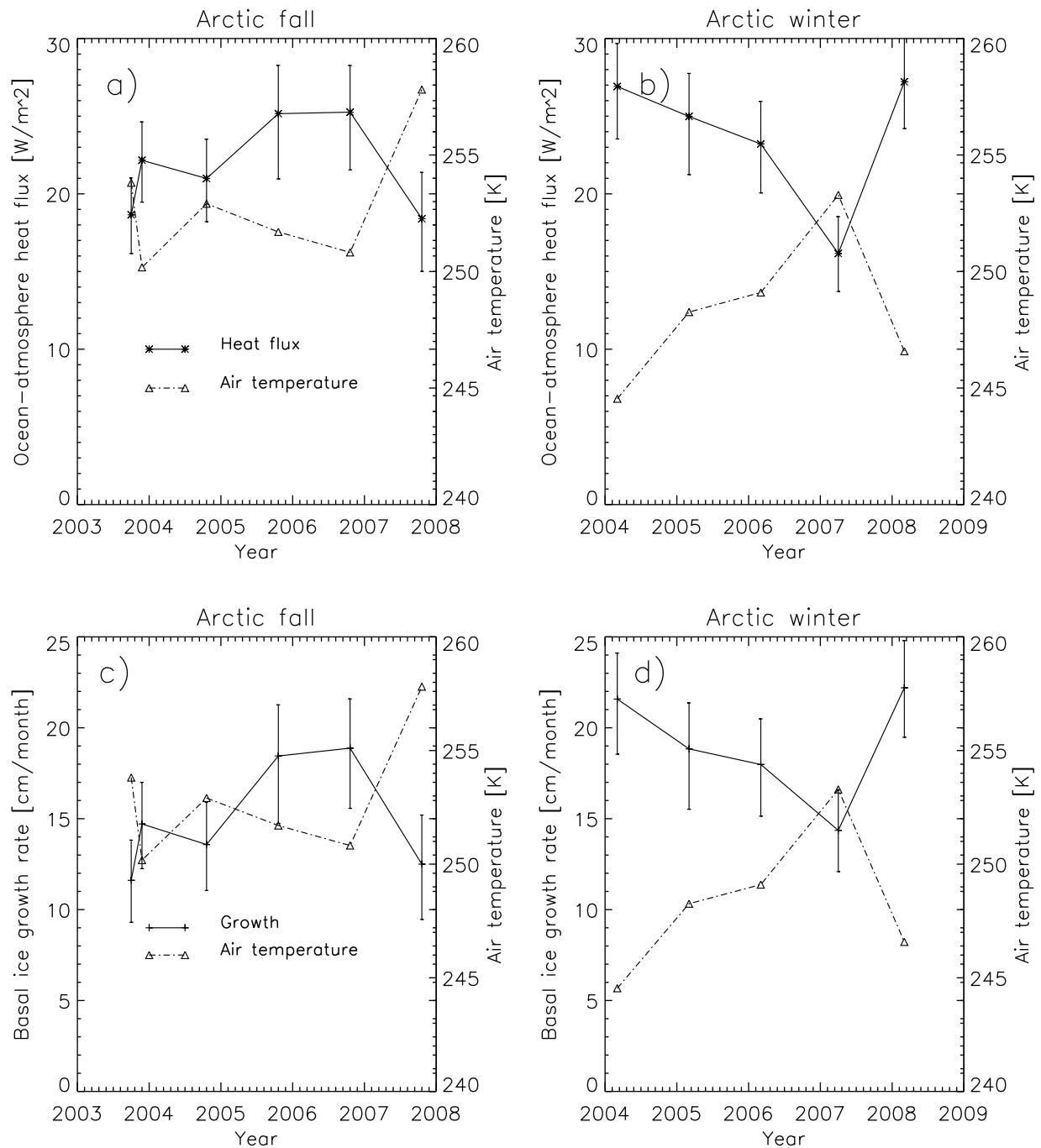


Figure 6. The mean ocean-atmosphere heat flux, basal ice growth rate, and 2 m air temperature for ice-covered regions during the Arctic fall and winter seasons.

effective insulation, growth of the sea ice and the addition of snow over the fall and early winter limited increases to the winter heat flux. The MA07 results show a lower equivalent heat flux than FM04 which is due to the additional time for growth for the thin ice classes which reduces the overall heat flux. The FM08 results suggest that an increase in the ocean-atmosphere heat flux may be beginning to appear in the winter due to the large decrease in ice and snow thickness (effective insulation), however this cannot be fully determined here due to uncertainties in the input parameters.

4.3. East and West Arctic Differences

[41] Sections 4.1 and 4.2.2 showed that ice thickness and energy exchange for the ice-covered regions of the Arctic Ocean experienced changes for the 2003–2008 time period, however certain regions of the Arctic were impacted differently than others. Here we discuss the regional impact of such changes by dividing the Arctic into two regions, East Arctic (0° – 180° longitude) and West Arctic (180° – 360° longitude), for the purpose of studying the regional variability of ice thickness, energy exchange, and ice growth.

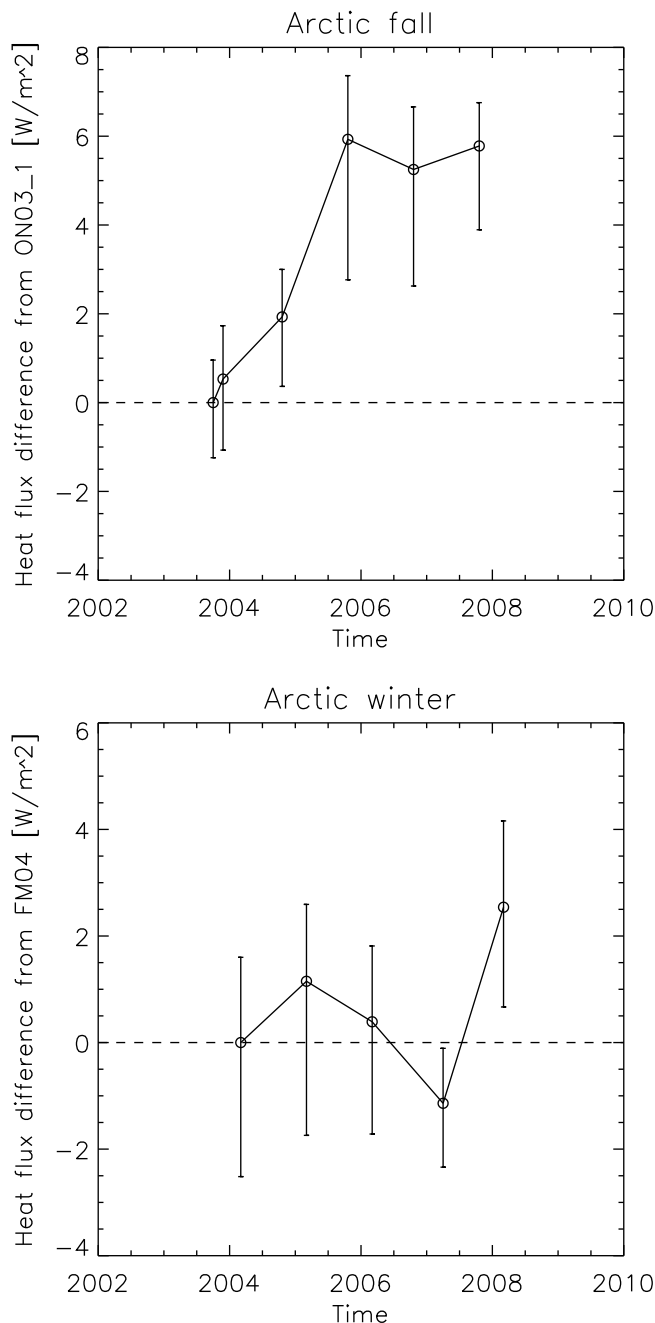


Figure 7. Ocean-atmosphere heat flux differences for the different time periods under the same meteorological conditions, differences are relative to the first campaign of the season. The error bars for the heat flux differences are taken from the combined uncertainties from the freeboard, snow depth, snow density, and ice density uncertainties discussed in section 4.2.1.

The regional ice thickness distributions, mean surface air temperatures, and mean growth rates are discussed. The mean growth rate and heat flux terms are used interchangeably here since the two are closely related.

[42] Figure 8 shows a large decline in the amount of thick ice (>3 m) in both regions during the fall periods, with the East Arctic showing a particularly steep decline in 2005.

Much of the ice of thickness greater than 3 m was replaced by ice 0.4–1.6 m thick, with large increases in the 0.2–0.8 m ice thickness class in the East Arctic. Both regions experienced similar variabilities in the surface air temperature, but differences in growth rate variabilities can be seen between the eastern and western Arctic regions due to differences in the ice thickness distribution. In 2005 and 2006 the East Arctic region experienced sharp increases in the ice growth rate/heat flux compared to the ON03_1 period (which had a lower surface air temperature) due largely to the increased amount of 0.2–0.8 m thick ice. The West Arctic region experienced similar, but less prominent, increases in the ice growth/heat flux in 2005 and 2006 due to the loss of thick ice >3 m.

[43] Figure 9 shows the regional thickness distributions, ice growth rate, and surface air temperature for the winter periods. The East Arctic winter time periods also experienced a general decline in the percentage of thick ice >3 m while the West Arctic did not see large changes in the ice thickness distribution until 2008. Despite losses in the thickest ice category as well as the overall mean ice thickness, the ice growth rate/heat flux is similar for the respective regions with similar surface air temperatures. Thus, as was observed in section 4.2 for the ice-covered Arctic, most of the winter time variability in ice growth rates appears to be due to changes in surface air temperature rather than due to changes in the ice thickness distribution.

5. Results for the Full Arctic Ocean

[44] Section 4 showed changes to the ocean-atmosphere heat flux and ice growth rate for areas containing ICESat data. We now extend the analysis to the full Arctic Ocean, including open water areas, to better place the results into context given the large changes in sea ice areal coverage over the time period.

[45] In this section, the heat flux and ice growth rates are calculated for nonice-covered areas by using sea surface temperature data described in section 2. Areas with an ice concentration greater than 0 and less than 30% were treated initially as open water, but with a sea surface temperature at the freezing point of sea water. For the nonice-covered areas, the ice growth rate and ocean-atmosphere heat flux were calculated at 6 h time intervals. If the sea surface temperature was at the freezing point the ice was allowed to grow in thickness and the growth rate was approximated from the net surface heat flux and equation 10, if the sea surface temperature was greater than freezing point of sea water then the ice thickness and growth rates were set to 0. Without the insulation of a sea ice cover, the net surface heat flux tended to be much larger than that from the ice-covered regions. However, the rate of ice growth rate is not directly proportional to the net surface heat flux in nonice-covered areas because of the limitation that ice will only grow once the surface temperature has reached the freezing point.

[46] To determine the net heat output and ice production of the Arctic Ocean, we first grid the heat flux and ice growth rate data onto a 25 km polar stereographic grid. Gaps in the gridded data were filled in through the use of a Gaussian smoother with a 20 km length scale (following Kwok *et al.* [2009]). Ice-covered and nonice-covered areas were filled in independently using their respective data sets. The pole

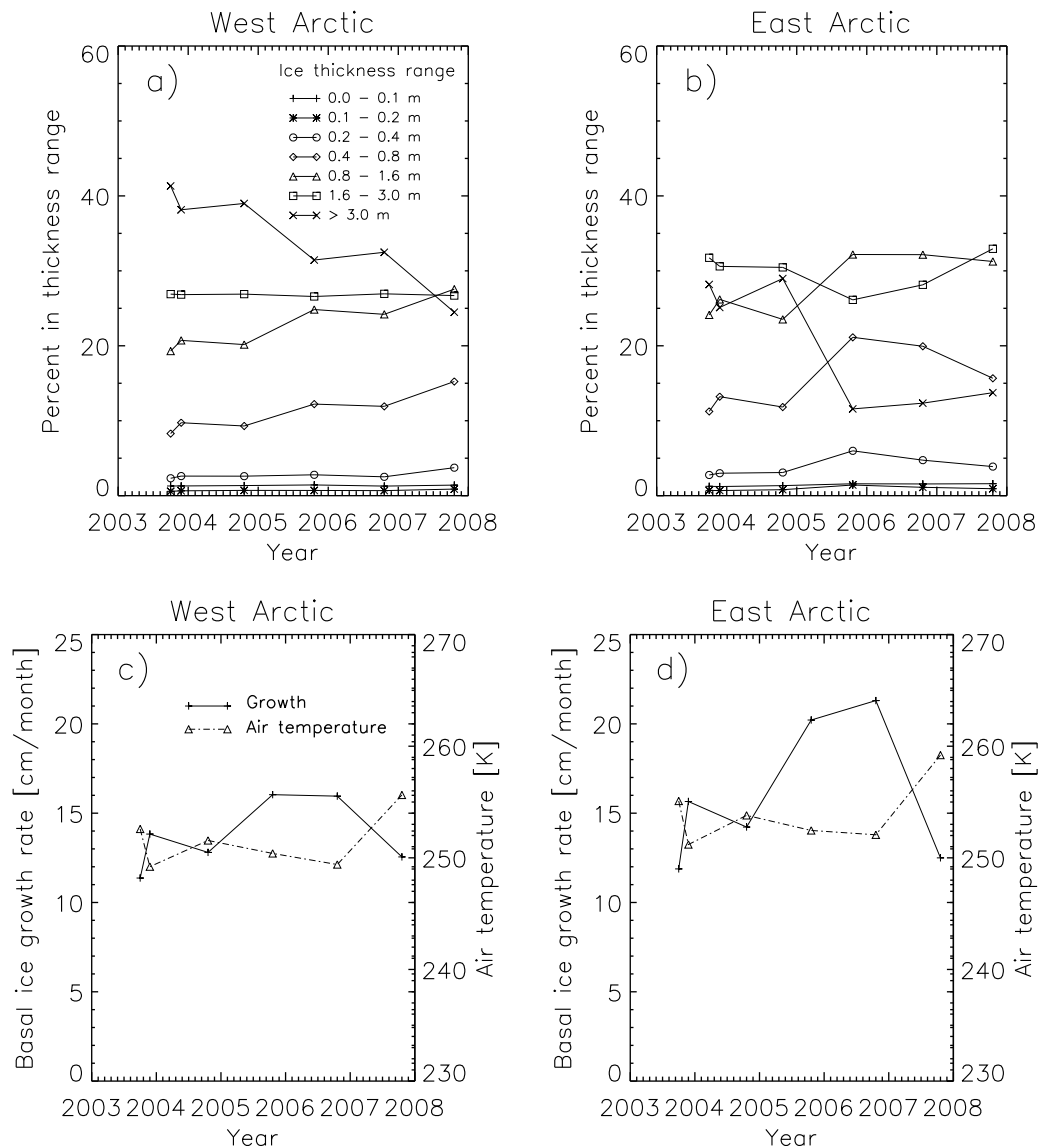


Figure 8. Fall time period ice thickness distributions, mean basal ice growth rates, and mean surface air temperatures for the ice-covered east and west Arctic regions.

hole north of 86 degrees was not filled in due to the large uncertainty introduced in interpolating the data over such a large region. The total area of the Arctic Ocean considered in this section for all time periods is $6.47 \times 10^6 \text{ km}^2$. The net surface heating rate and net ice volume production are this area value multiplied by the ocean-atmosphere heat flux and ice growth rates, respectively. Results for the net surface heating rate and ice volume production as well as the areal coverage of ice and nonice areas are shown in Figure 10.

5.1. Net Arctic Ocean Heat Output

[47] Figure 10c shows an increasing trend in the total Arctic Ocean heating rate for the fall periods, while Figure 10d shows comparatively little change in the winter heating rate. Figures 10a and 10d show that for sea ice-covered regions, the net heating rate did not change markedly compared to the full Arctic Ocean domain in both the fall and winter. The heating rate over nonice-covered areas

changed most dramatically in 2007 due to the larger amount of open water in that year (Figures 10b and 10e), increasing by nearly a factor of 5 from the previous years. Though ice-covered areas made up the dominant portion of the Arctic Ocean, the total heating rates were nearly equal over ice-covered and nonice-covered areas for the fall periods (with the exception of 2007). In 2004, 2005, and 2006 the net heating rate increased by 44%, 17%, and 12% from 2003, respectively. While in 2007 the large increase in nonice-covered areal coverage caused the total heating rate for the Arctic Ocean to increase by 300% from that in 2003. With the exception of the much later MA07 measurement time period, there was much less change in the winter time heating rates with a maximum change of 16% observed.

[48] The results show an overall increase in the amount of ocean-atmosphere heat transfer in the fall periods. Section 4.2.2 showed that independent of changes in meteorological conditions, thinning of the sea ice cover is

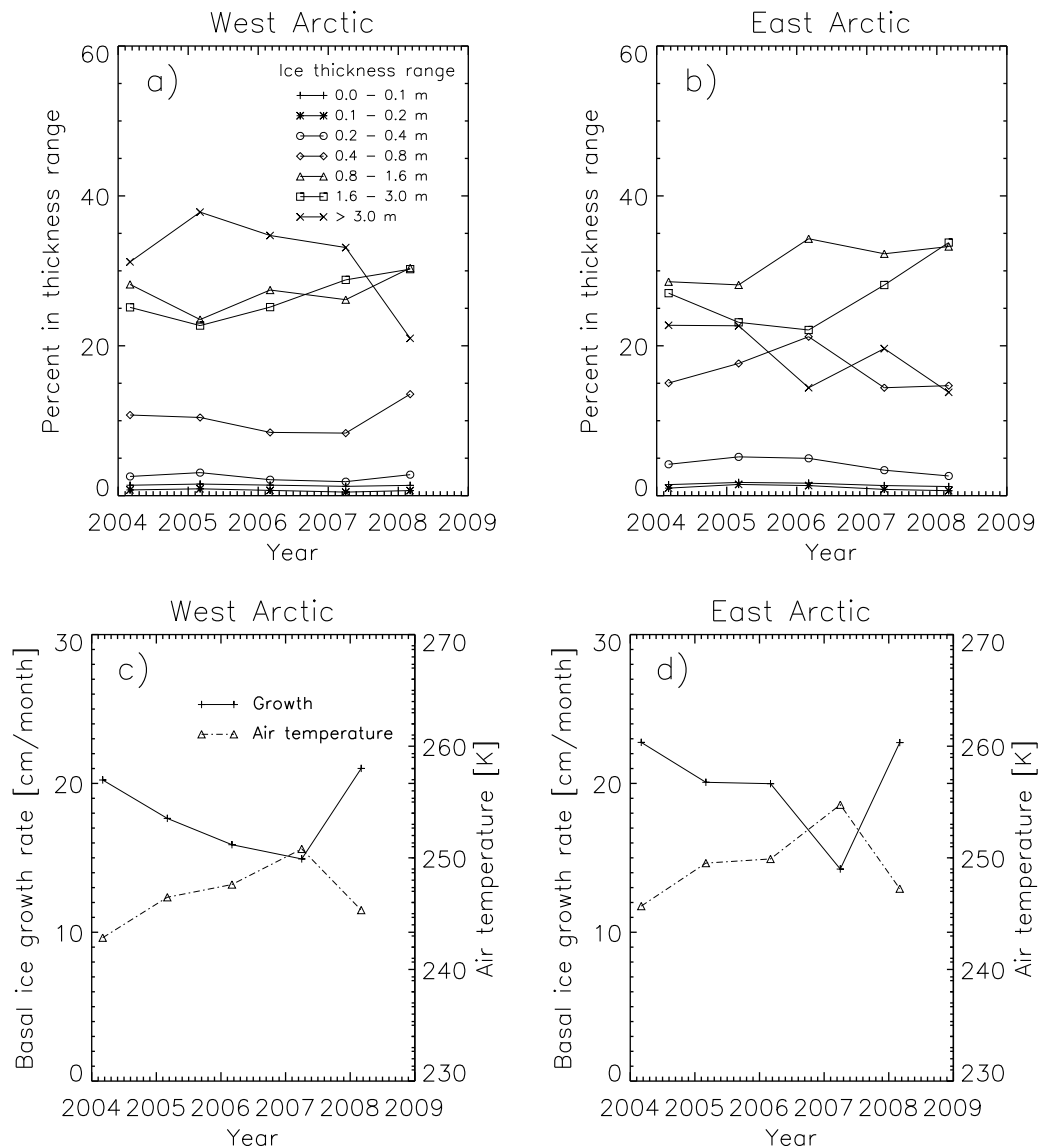


Figure 9. Winter time period ice thickness distributions, mean basal ice growth rates, and mean surface air temperatures for the ice-covered east and west Arctic regions.

responsible for up to a 40% increase in the net heat output in the ice-covered Arctic Ocean. However, this increase is small compared to the effect caused by changes in the ice areal coverage. The anomalously low areal coverage of sea ice in 2007 marked a turning point where the net Arctic Ocean heating rate became dominantly determined by the amount of ice-free area.

5.2. Net Arctic Ocean Ice Production

[49] The observed changes in sea ice thickness and ocean-atmosphere heat flux also lead to changes in the ice growth rate. Of particular interest is whether the observed losses in sea ice thickness and areal coverage led to a higher rate of ice production which could aid in the recovery of sea ice thickness and volume.

[50] For sea ice-covered regions, the mean basal ice growth rates are shown in Table 6. Though basal ice growth varied with time depending on the surface air temperature

and ice thickness distribution in a similar manner as the heat flux, Table 6 shows that a higher growth rate in the fall was generally followed by a lower growth rate in the winter and vice versa. The observed decreases in ice thickness may be due to a longer melt season as observed by *Markus et al.* [2009], increased oceanic heat flux as observed for the western Arctic by *Woodgate et al.* [2010], and/or increased ice export rather than due to changes in ice growth. These observations show that an expected increased basal ice growth rate associated with decreasing ice thickness did not largely occur over the 2003–2008 time period mainly due to associated changes in the surface air temperature.

[51] The rate of ice volume production for ice-covered and nonice-covered areas is shown in Figure 10, the production of ice can be seen to vary considerably from year to year. For the fall season ice-covered portion of the Arctic Ocean, the production of ice peaked in 2005 and 2006 due in part to the thinning of the ice cover and associated

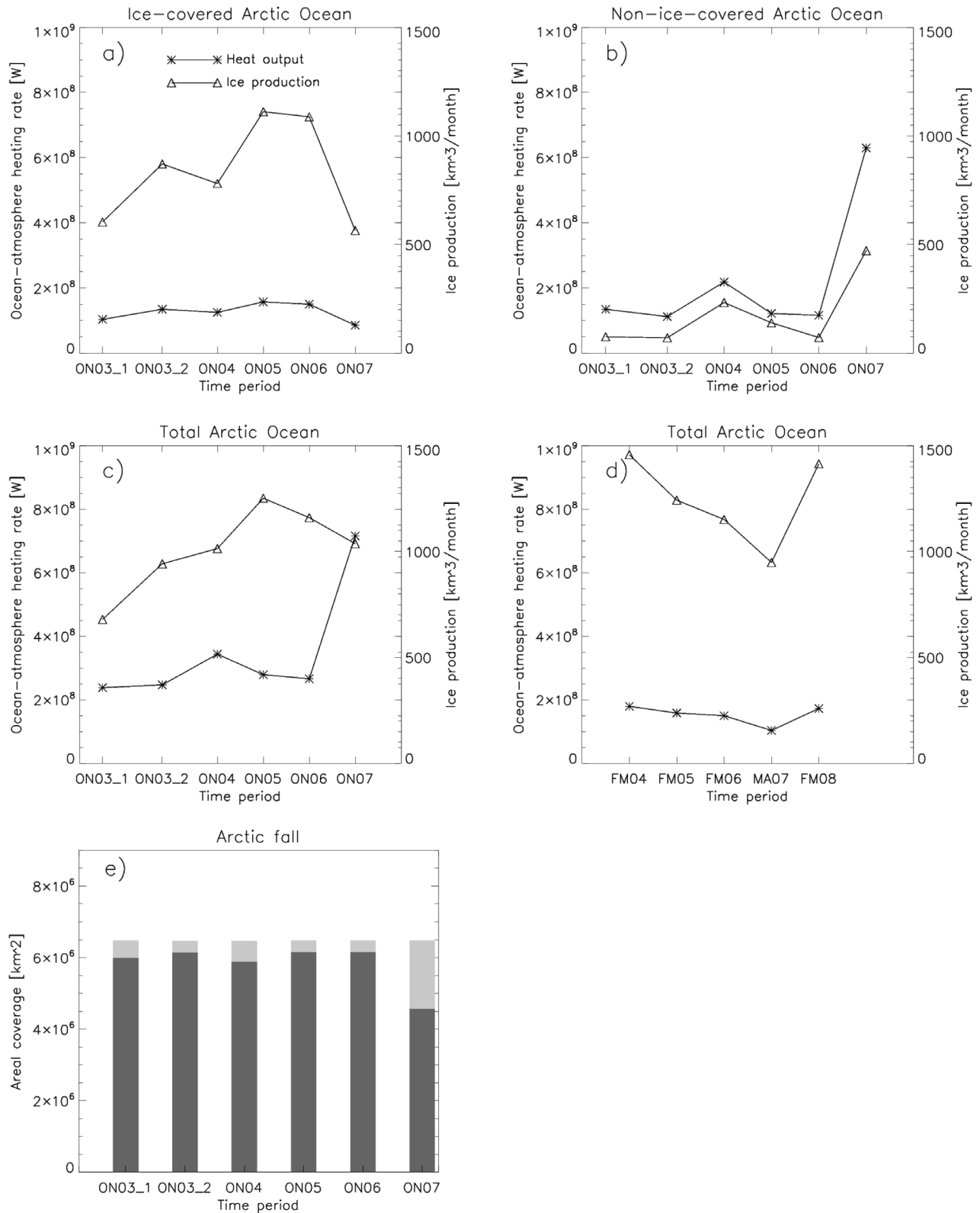


Figure 10. Net ocean-atmosphere heating rate and ice volume production for the (a) ice-covered, (b) nonice-covered, and (c and d) total Arctic Ocean. (e) The dark colored bars represent the areal coverage of ice-covered regions, and the light colored bars represent the nonice-covered areal coverage. For the winter time periods, all regions are ice covered. The total area of the Arctic Ocean domain for all time periods in this study is $6.47 \times 10^6 \text{ km}^2$.

Table 6. Basal Ice Growth Rate for Ice-Covered Regions During the Fall and Winter Seasons^a

	2003–2004	2004–2005	2005–2006	2006–2007	2007–2008
Fall ice growth (cm month ⁻¹)	10.1 (14.2)	13.3	18.1	17.7	12.4
Winter ice growth (cm month ⁻¹)	22.6	19.2	17.8	14.7	21.9

^aThe ON03_2 period is shown in parentheses.

increased ocean-atmosphere heat flux discussed in section 4. In 2007, the production of ice in ice-covered regions reached the lowest point due to the high surface air temperatures and low ice areal coverage of the time period, while in nonice-covered areas the ice production increased by nearly a factor of 3 compared to the previous fall seasons.

[52] For the full Arctic Ocean fall periods, the combination of ice production in ice-covered and nonice-covered areas led to a peak in the ice production in 2005 and a decrease in the following years. Despite the large increase in total ocean-atmosphere heat output in 2007, warm ocean and air temperatures kept the level of ice production near to that of 2004. Thus, the 2007 ice minimum led to a greatly increased release of heat from the ocean to the atmosphere, however this increased heating rate did not lead to an increase in overall ice production because the ocean had yet to cool to the freezing point. The winter period ice production was much less variable, excluding the much later MA07 measurement period the ice production varied by less than 20% over the 2004–2008 time period. The winter time ice production variability was driven primarily by variability in the surface air temperature.

6. Summary and Discussion

[53] In this study we have combined ICESat freeboard retrievals with a snow depth model to estimate snow and sea ice thickness values for the Arctic Ocean during the 2003–2008 fall and winter time periods. The thickness data were used with meteorological data and a thermodynamic sea ice model to calculate the turbulent, radiative, and conductive heat fluxes, as well as the total ocean-atmosphere heat output and ice volume production for the Arctic Ocean. Sensitivities to the input parameters were determined and used to estimate the error in the calculated ocean-atmosphere heat fluxes and ice growth rates. The main factor affecting the uncertainty in our results was found to be uncertainties in the surface air temperature. Laser altimetry data was found to be particularly useful for determining the heat fluxes since the results are relatively insensitive to snow depth errors.

[54] The heat flux and ice growth rates in ice-covered regions presented here are consistent with those from previous observational studies conducted on multiyear ice. The advantage of the data sets used in this study is that they allow for estimates of heat flux over the entire Arctic basin. Also in agreement with the results of previous studies [e.g., Kwok *et al.*, 2009; Giles *et al.*, 2008; Maslanik *et al.*, 2007], this study shows that during the 2003–2008 time period the mean Arctic sea ice thickness decreased with much of the thickest ice (>3 m) being replaced by ice 0.8–3.0 m thick. Variability in the calculated ocean-atmosphere heat flux and basal ice growth for ice-covered regions was primarily driven by changes in the surface air temperature as well as by the observed changes in the ice thickness distribution.

Heat fluxes during the fall periods were more sensitive to changes in the ice thickness distribution, with the eastern Arctic experiencing the greatest change in ice growth and heat flux due to changes in the ice thickness distribution. Taking variations in meteorological conditions into account, the fall period ocean-atmosphere heat fluxes were found to be greatly increased in 2005, 2006, and 2007 compared to 2003 due to thinning of the sea ice cover. The winter time heat fluxes were much more impacted by changes in the surface air temperature rather than changes in the ice thickness distribution. Although the mean ice thickness decreased over the 2004–2008 winter time periods, the winter effective insulation did not largely change until 2008 at which time it experienced a large decline of nearly 1 m in effective sea ice thickness. The large decline in the winter 2008 effective insulation is also associated with an increase in the heat flux after differences in meteorological forcings are taken into account, though this increase is not as prominent as that observed in the fall and is within the estimated uncertainty.

[55] For the whole of the Arctic Ocean, this study shows that increases in the net ocean-atmosphere heat output have occurred due to thinning and area (volume) loss of the Arctic sea ice cover. However, a remaining question is: what magnitude of changes to the surface air temperature have occurred due to this decrease in sea ice volume and associated increase in the ocean-atmosphere heat flux? Surface air temperatures in the Arctic are highly variable so quantifying the impact of a changing sea ice cover on surface air temperatures is difficult [Serreze and Francis, 2006]. Serreze *et al.* [2009] show that decreases in the areal extent of Arctic are tied to increased surface air temperatures for the 1979–2007 fall seasons, but that this effect is not largely present during the winter season. The increased surface air temperatures in the fall were found to be due to a surface heating source and attributed to an increased surface heat flux. This study shows that over the 2003–2008 time period losses in both ice thickness and areal coverage did indeed lead to an overall increase in the surface heat flux. Despite large losses in ice thickness and effective insulation, changes in ice areal coverage were found to be the dominant factor in impacting the surface heat flux. Most notably, the anomalously low areal coverage of sea in the fall of 2007 led to an ocean-atmosphere heat output nearly 3 times higher than that from previous years.

[56] Serreze *et al.* [2009] also note that slight warming may also be beginning to appear in the winter time. They state this may be due to delays in autumn freezeup, but eventually decreased ice extent and thickness in the winter will also begin to play a role. Delays in autumn freezeup have been observed by Markus *et al.* [2009]. However, this study shows that though there was a decrease in the mean thickness and amount of thick (>3 m) ice in the winter, these changes did not lead to a large change in the ocean-atmosphere heating rate since it is less sensitive to changes in the amount of

thick ice. It appears that a surface warming signal associated with a thinning sea ice cover could just be beginning to emerge in the winter, but future observations will be required to determine whether this effect becomes stronger and more significant with time.

[57] Overall, these results show that the decreasing volume of the Arctic sea ice cover has led to a decreasing ability to insulate the atmosphere from the relatively warm underlying ocean. This effect is currently most pronounced in the fall, with the winter being less affected as the ice has sufficiently thickened to a point where the ocean-atmosphere heat flux is less sensitive to changes in the ice thickness. These increased heat fluxes in the fall periods likely played a role in increasing surface air temperatures in the Arctic. Though this data set spans only 5 years, it was collected at a time when large losses in sea ice thickness and areal extent were observed. The continuation of large-scale sea ice thickness measurements from future airborne and satellite missions such as NASA's Operation IceBridge and the planned ICESat-2 mission, as well as ESA's CryoSat-2 mission, will be vital to understanding future changes to the sea ice cover and its impact on the climate.

[58] A major limitation in this study of the Arctic ocean-atmosphere heat flux and ice growth rate is the irregular time sampling and limited temporal availability of ICESat data. Future satellite altimetry missions will maintain year-round data collection for improved observation of year-to-year variations. For the currently available ICESat data, it would be useful to combine the observational data with model data using an assimilation approach. Doing so would enable a better understanding of reasons for the large losses in ice volume over the time period, how annual ice production was affected by the observed changes, and how an increased ocean-atmosphere heat flux from a reduced ice cover affected surface air temperatures throughout the whole of the Arctic.

[59] **Acknowledgments.** The authors would like to thank two anonymous reviewers for their invaluable suggestions, which helped in improving the manuscript. The ECMWF data for this study are from the Research Data Archive (RDA), which is maintained by the Computational and Information Systems Laboratory (CISL) at the National Center for Atmospheric Research (NCAR). NCAR is sponsored by the National Science Foundation (NSF). The original data are available from the RDA (<http://dss.ucar.edu>) in data set number ds627.0. We also acknowledge NSIDC for providing the AMSR-E and ICESat data used in this study (<http://nsidc.org/>).

References

- Ackerman, S. A., R. E. Holz, R. Frey, E. W. Eloranta, B. C. Maddux, and M. McGill (2008), Cloud detection with MODIS. Part II: Validation, *J. Atmos. Oceanic Tech.*, *25*, 1073–1086.
- Arctic Climate Impact Assessment (2005), *Arctic Climate Impact Assessment*, 1042 pp., Cambridge Univ. Press, Cambridge, U. K.
- Boé, J., A. Hall, and X. Qu (2009), Current GCMs' unrealistic negative feedback in the Arctic, *J. Clim.*, *22*, 4682–4695.
- Comiso, J. C., C. L. Parkinson, R. Gersten, and L. Stock (2008), Accelerated decline in the Arctic sea ice cover, *Geophys. Res. Lett.*, *35*, L01703, doi:10.1029/2007GL031972.
- Farrell, S. L., S. W. Laxon, D. C. McAdoo, D. Yi, and H. J. Zwally (2009), Five years of Arctic sea ice freeboard measurements from the Ice, Cloud and land Elevation Satellite, *J. Geophys. Res.*, *114*, C04008, doi:10.1029/2008JC005074.
- Giles, K. A., S. W. Laxon, and A. L. Ridout (2008), Circumpolar thinning of Arctic sea ice following the 2007 record ice extent minimum, *Geophys. Res. Lett.*, *35*, L22502, doi:10.1029/2008GL035710.
- Hack, J. J., B. A. Boville, B. P. Briegleb, J. T. Kiehl, P. J. Rasch, and D. L. Williamson (1993), Description of the NCAR Community Climate Model (CCM2), *Tech. Note TN-382+STR*, 108 pp., Natl. Cent. for Atmos. Res., Boulder, Colo.
- Key, J. R., R. A. Silcox, and R. S. Stone (1996), Evaluation of surface radiative flux parameterizations for use in sea ice models, *J. Geophys. Res.*, *101*, 3839–3849.
- Kovacs, A. (1996), Sea ice: Part II. Estimating the full-scale tensile, flexural, and compressive strength of first-year ice, *Rep. 96-11*, Cold Reg. Res. and Eng. Lab., Hanover, N. H.
- Kurtz, N. T., T. Markus, D. J. Cavalieri, W. Krabill, J. G. Sonntag, and J. Miller (2008), Comparison of ICESat data with airborne laser altimeter measurements over Arctic sea ice, *IEEE Trans. Geosci. Remote Sens.*, *46*, 1913–1924.
- Kurtz, N. T., T. Markus, D. J. Cavalieri, L. C. Sparling, W. B. Krabill, A. J. Gasiewski, and J. G. Sonntag (2009), Estimation of sea ice thickness distributions through the combination of snow depth and satellite laser altimetry data, *J. Geophys. Res.*, *114*, C10007, doi:10.1029/2009JC005292.
- Kwok, R., and G. F. Cunningham (2008), ICESat over Arctic sea ice: Estimation of snow depth and ice thickness, *J. Geophys. Res.*, *113*, C08010, doi:10.1029/2008JC004753.
- Kwok, R., G. F. Cunningham, H. J. Zwally, and D. Yi (2007), Ice, Cloud, and land Elevation Satellite (ICESat) over Arctic sea ice: Retrieval of freeboard, *J. Geophys. Res.*, *112*, C12013, doi:10.1029/2006JC003978.
- Kwok, R., G. F. Cunningham, M. Wensnahan, I. Rigor, H. J. Zwally, and D. Yi (2009), Thinning and volume loss of the Arctic Ocean sea ice cover: 2003–2008, *J. Geophys. Res.*, *114*, C07005, doi:10.1029/2009JC005312.
- Laevastu, T. (1960), Factors affecting the temperature of the surface layer of the sea, *Comment. Phys. Math.*, *25*, 128–134.
- Lindsay, R. W. (1998), Temporal variability of the energy balance of thick Arctic pack ice, *J. Clim.*, *11*, 313–333.
- Liu, A. K., and D. J. Cavalieri (1998), Sea-ice drift from wavelet analysis of DMSP SSM/I data, *Int. J. Remote Sens.*, *19*, 1415–1423.
- Lupkes, C., T. Vihma, E. Jakobson, G. König-Langlo, and A. Tetzlaff (2010), Meteorological observations from ship cruises during summer to the central Arctic: A comparison with reanalysis data, *Geophys. Res. Lett.*, *37*, L09810, doi:10.1029/2010GL042724.
- Manabe, S., and R. J. Stouffer (1980), Sensitivity of a global climate model to an increase of CO₂ in the atmosphere, *J. Geophys. Res.*, *85*, 5529–5554.
- Markus, T., J. C. Stroeve, and J. Miller (2009), Recent changes in Arctic sea ice melt onset, freeze-up, and melt season length, *J. Geophys. Res.*, *114*, C12024, doi:10.1029/2009JC005436.
- Maslanik, J. A., C. Fowler, J. Stroeve, S. Drobot, J. Zwally, D. Yi, and W. Emery (2007), A younger, thinner Arctic ice cover: Increased potential for rapid, extensive sea-ice loss, *Geophys. Res. Lett.*, *34*, L24501, doi:10.1029/2007GL032043.
- Maykut, G. A. (1978), Energy exchange over young sea ice in the central Arctic, *J. Geophys. Res.*, *83*, 3646–3658.
- Maykut, G. A. (1982), Large-scale heat exchange and ice production in the central Arctic, *J. Geophys. Res.*, *87*, 7971–7984.
- Maykut, G. A., and P. E. Church (1973), Radiation climate of Barrow, Alaska, 1962–66, *J. Appl. Meteorol.*, *12*, 620–628.
- Maykut, G. A., and D. K. Perovich (1987), The role of shortwave radiation in the summer decay of a sea ice cover, *J. Geophys. Res.*, *92*, 7032–7044.
- Maykut, G. A., and N. Untersteiner (1969), Numerical prediction of the thermodynamic response of Arctic sea ice to environmental changes, *Doc. RM-6093-PR*, Rand Corp., Santa Monica, Calif.
- Parkinson, C. L., and W. M. Washington (1979), A large-scale numerical model of sea ice, *J. Geophys. Res.*, *84*, 311–337.
- Pease, C. H. (1987), The size of wind-driven coastal polynyas, *J. Geophys. Res.*, *92*, 7049–7059.
- Perovich, D. K., T. C. Grenfell, J. A. Richter-Menge, B. Light, W. B. Tucker III, and H. Eicken (2003), Thin and thinner: Sea ice mass balance measurements during SHEBA, *J. Geophys. Res.*, *108*(C3), 8050, doi:10.1029/2001JC001079.
- Persson, P. O. G., C. W. Fairall, E. L. Andreas, P. S. Guest, and D. K. Perovich (2002), Measurements near the Atmospheric Surface Flux Group tower at SHEBA: Near surface conditions and surface energy budget, *J. Geophys. Res.*, *107*(C10), 8045, doi:10.1029/2000JC000705.
- Rigor, I. G., J. M. Wallace, and R. L. Colony (2002), Response of sea ice to the Arctic oscillation, *J. Clim.*, *15*, 2648–2663.
- Rothrock, D. A., D. B. Percival, and M. Wensnahan (2008), The decline in Arctic sea-ice thickness: Separating the spatial, annual, and interannual variability in a quarter century of submarine data, *J. Geophys. Res.*, *113*, C05003, doi:10.1029/2007JC004252.
- Semtner, A. J., Jr. (1976), A model for the thermodynamic growth of sea ice in numerical investigations of climate, *J. Phys. Oceanogr.*, *6*, 379–389.
- Serreze, M. C., and J. A. Francis (2006), The Arctic amplification debate, *Clim. Change*, *76*, 241–264.

- Serreze, M. C., A. P. Barrett, J. C. Stroeve, D. N. Kindig, and M. M. Holland (2009), The emergence of surface-based Arctic amplification, *Cryosphere*, *3*, 11–19.
- Shine, K. P. (1984), Parameterization of shortwave flux over high albedo surfaces as a function of cloud thickness and surface albedo, *Q. J. R. Meteorol. Soc.*, *110*, 747–764.
- Stark, J. D., C. J. Donlon, M. J. Martin, and M. E. McCulloch (2007), Ostia: An operational, high resolution, real time, global sea surface temperature analysis system, paper presented at Oceans '07, Inst. of Electr. and Electr. Eng., Aberdeen, U. K.
- Steele, M., and T. Boyd (1998), Retreat of the cold halocline layer in the Arctic Ocean, *J. Geophys. Res.*, *103*, 10,419–10,435.
- Stroeve, J., M. Serreze, S. Drobot, S. Gearheard, M. Holland, J. Maslanik, W. Meier, and T. Scambos (2008), Arctic sea ice extent plummets in 2007, *EOS Trans. AGU*, *89*(2), 13–14, doi:10.1029/2008EO020001.
- Sturm, M., D. K. Perovich, and J. Holmgren (2002), Thermal conductivity and heat transfer through the snow on the ice of the Beaufort Sea, *J. Geophys. Res.*, *107*(C21), 8043, doi:10.1029/2000JC000409.
- Wadhams, P., W. B. Tucker III, W. B. Krabill, R. N. Swift, J. C. Comiso, and N. R. Davis (1992), Relationship between sea ice freeboard and draft in the Arctic basin, and implications for ice thickness monitoring, *J. Geophys. Res.*, *97*, 20,325–20,334.
- Warren, S. G., I. G. Rigor, N. Untersteiner, V. F. Radionov, N. N. Bryazgin, Y. I. Aleksandrov, and R. Colony (1999), Snow depth on Arctic sea ice, *J. Clim.*, *12*, 1814–1829.
- Weeks, W. F., and O. S. Lee (1958), Observations on the physical properties of sea ice at Hopedale, Labrador, *Arctic*, *11*, 92–108.
- Weller, G. (1972), Radiation flux investigation, *AIDJEX Bull.*, *14*, 28–30.
- Wentz, F., and T. Meissner (2000), AMSR ocean algorithm theoretical basis document, version 2, report, Remote Sens. Syst., Santa Rosa, Calif.
- Wentz, F., and T. Meissner (2004), AMSR-E/Aqua Daily L3 Global Ascending/Descending .25 × .25 deg Ocean Grids, V002, October 2003 to March 2008, http://nsidc.org/data/ae_dyocn.html, Natl. Snow and Ice Data Cent., Boulder, Colo. (Updated daily.)
- Woodgate, R. A., T. Weingartner, and R. Lindsay (2010), The 2007 Bering Strait oceanic heat flux and anomalous Arctic sea-ice retreat, *Geophys. Res. Lett.*, *37*, L01602, doi:10.1029/2009GL041621.
- Zwally, H. J., et al. (2002), ICESat's laser measurements of polar ice, atmosphere, ocean, and land, *J. Geodyn.*, *24*, 405–445.

L. N. Boisvert, S. L. Farrell, N. T. Kurtz, T. Markus, and D. L. Worthen, Hydrospheric and Biospheric Sciences Laboratory, NASA Goddard Space Flight Center, 8800 Greenbelt Rd., MS 614.1, Greenbelt, MD 20771, USA. (nathan.t.kurtz@nasa.gov)